Ph.D. DISSERTATION

Low-Complexity PTS Schemes Using Dominant Time-Domain Samples in OFDM Systems

OFDM 시스템에서의 PAPR 감소를 위한 시간 영역의 큰 샘플을 이용한 저복잡도 PTS 기법

BY

LEE KANG-SEOK

FEBRUARY 2018

DEPARTMENT OF ELECTRICAL ENGINEERING AND
COMPUTER SCIENCE
COLLEGE OF ENGINEERING
SEOUL NATIONAL UNIVERSITY

Ph.D. DISSERTATION

Low-Complexity PTS Schemes Using Dominant Time-Domain Samples in OFDM Systems

OFDM 시스템에서의 PAPR 감소를 위한 시간 영역의 큰 샘플을 이용한 저복잡도 PTS 기법

BY

LEE KANG-SEOK

FEBRUARY 2018

DEPARTMENT OF ELECTRICAL ENGINEERING AND
COMPUTER SCIENCE
COLLEGE OF ENGINEERING
SEOUL NATIONAL UNIVERSITY

Low-Complexity PTS Schemes Using Dominant Time-Domain Samples in OFDM Systems

OFDM 시스템에서의 PAPR 감소를 위한 시간 영역의 큰 샘플을 이용한 저복잡도 PTS 기법

지도교수 노 종 선

이 논문을 공학박사 학위논문으로 제출함

2018년 2월

서울대학교 대학원

전기 컴퓨터 공학부

이 강 석

이강석의 공학박사 학위 논문을 인준함

2018년 2월

위 원 장: _____
부위원장: _____
위 원: _____
위 원: _____
위 원: _____

Abstract

In orthogonal frequency division multiplexing (OFDM) systems, high peak-to-average power ratio (PAPR) of OFDM signals is one of the most important problems. The high PAPR of OFDM signals causes serious nonlinear distortions in process of passing through high power amplifier (HPA). These distortions have a effect on in-band distortion and out-of-band radiation, which result in bit error rate degradation of received OFDM signals and interference in adjacent channel, respectively. In order to solve the PAPR problem of OFDM signals, various PAPR reduction schemes have been proposed.

This dissertation includes research results on a kind of the PAPR reduction schemes, called the partial transmit sequence (PTS) for the OFDM systems. As a solution to the PAPR problem in OFDM systems, the PTS scheme is a fairly suitable scheme due to its PAPR reduction performance and distortionless characteristics. The PTS scheme generates several candidate OFDM signals to represent an original OFDM signal and selects one with the lowest PAPR among them for transmission. However, a serious problem in the PTS scheme is high computational complexity, which is mainly required to generate and process the candidate OFDM signals. In this dissertation, in an effort to reduce its computational complexity, new PTS schemes are proposed using dominant time-domain samples of OFDM signals. Dominant time-domain samples is a small number of samples of OFDM signals used to estimate PAPRs of candidate OFDM signals efficiently.

In the first part of this dissertation, low-complexity PTS schemes are proposed using new selection methods of dominant time-domain samples. The proposed selection methods of dominant time-domain samples are based on selection methods of candidate samples in candidate OFDM signals. These methods select dominant time-domain samples with reduced computational complexity. The dominant time-domain samples

selected by the proposed methods are used to estimate PAPRs of candidate OFDM signals with high accuracy. Therefore, the proposed low-complexity PTS schemes can achieve the optimal PAPR reduction performance with considerably reduced computational complexity.

In the second part of this dissertation, improved PTS schemes are proposed to lower the computational complexity of previous PTS schemes further while maintaining high performance of PAPR reduction. Similar with the PTS schemes proposed in the previous part of this dissertation, the improved PTS schemes utilize dominant time-domain samples and candidate samples. However, they use more efficient methods, which select the candidate samples by adaptive method or multi-stage method to select dominant time-domain samples. Therefore, the improved PTS schemes reduce computational complexity further while maintaining the optimal PAPR reduction performance.

The proposed PTS schemes in this dissertation use efficient methods to select dominant time-domain samples and thus they reduce the computational complexity considerably compared to previous PTS schemes. In addition, they achieve the optimal PAPR reduction performance, which is equivalent to that of the conventional PTS scheme with the low complexity. Due to the high performance and low complexity, they are fully expected to be used in the practical implementation of OFDM systems.

keywords: Dominant time-domain samples, Orthogonal frequency division multiplexing (OFDM), Partial transmit sequence (PTS), Peak-to-average power ratio (PAPR)
student number: 2012-20821

Contents

List of Tables

List of Figures

Chapter 1

INTRODUCTION

1.1 Introduction

Since high data transmission is required in wireless communication systems, a multi-carrier modulation (MCM) technique has recently attracted attention of wireless communication systems. The main idea of an MCM system is to split a high-rate data stream into several low-rate data streams and to modulate them by a set of parallel sub-carriers that makes full use of the available bandwidth. When the channel introduces inter-symbol interference (ISI), the MCM scheme does not require a complex equalizer at the receiver. It is a useful property when dealing with high-rate data stream in the time dispersive channel. From a time-domain perspective, this translates the wide-band transmission system into a collection of parallel narrow-band transmission systems, each operating at a lower data rate. From the frequency domain perspective, it transforms the frequency selective channel, i.e., non-flat spectrum across the frequency band of interest, into a collection of approximately flat sub-channels over which the data are transmitted in parallel. Thus, the MCM scheme has become one of the choices to combat the frequency selective fading channel.

Orthogonal frequency division multiplexing (OFDM) [1] is one of the most popular types of MCM schemes and an enhanced extension of frequency division multiplexing

(FDM). Since parallel sub-carriers have overlapped spectra, OFDM has high spectral efficiency and easy adaptation to severe channel without complex time-domain equalization. The wireless communication system using OFDM is robust against ISI and fading caused by multi-path propagation as well as narrow-band co-channel interference. In addition, the OFDM systems are efficient for hardware implementation because they can use the fast Fourier transform (FFT) instead of the discrete Fourier transform (DFT). Further, they have low sensitivity to time synchronization errors. Due to these valuable advantages, OFDM has been adopted as one of the most popular modulation techniques for wireless communications. OFDM has been used in the various applications, such as digital audio broadcasting (DAB), digital video broadcasting (DVB), digital multimedia broadcasting (DMB), wireless local area network (WLAN) IEEE 802.11 [2], long term evolution (LTE), and LTE advanced 4G mobile phone standards. OFDM is also a candidate for 5G cellular standard and military communication systems.

However, OFDM also has several disadvantages. The high peak-to-average power ratio (PAPR) of OFDM signals is one of the most serious problems in OFDM systems. Due to the nonlinear property of high power amplifier (HPA), the HPA output of OFDM signals with high PAPR causes in-band distortion and out-of-band radiation, which result in degradation of communication quality such as the bit error rate (BER). BER is an important performance evaluation criterion in all communication systems including OFDM systems in which high PAPR of the signal is a serious problem. Assuming that other system conditions such as channels and encoding/decoding schemes except only for PAPR reduction schemes are fixed in OFDM systems, BER is affected only by an employed PAPR reduction scheme and the corresponding PAPR. Therefore, good PAPR reduction performance means good BER performance, which evidently improves performance of communication systems.

In order to solve the PAPR problem in OFDM systems, various PAPR reduction schemes have been proposed [3, 4, 5, 6, 7, 8, 9, 10]. Clipping [3] is used to reduce the peak power by clipping the OFDM signals to the threshold level but it causes

severe in-band distortion and out-of-band radiation. To reduce the distortions caused by clipping, clipping and filtering (CAF) [4] is used, but filtering causes another distortion and increases computational complexity. Companding [5] scales time-domain signals nonlinearly such that signals with large amplitude are suppressed and signals with small amplitude are expanded, but it also distorts the signals unavoidably. Tone reservation (TR) [6] and active constellation extension (ACE) [7] change constellation points of some sub-carriers to reduce the PAPR, but their drawbacks are data rate loss and transmission power increase.

Selective mapping (SLM) [9] and partial transmit sequence (PTS) [10] schemes can effectively reduce the PAPR of OFDM signals without causing signal distortion. They require several inverse fast Fourier transform (IFFT) to generate candidate OFDM signals among which a candidate OFDM signal with the lowest PAPR is selected and then transmitted as the OFDM signal. In the OFDM system, since FFT and IFFT operations to generate and process OFDM signals, account for a substantial part of the overall computational complexity, IFFTs to generate candidate OFDM signals in SLM and PTS schemes can place a significant burden on the system. In general, PTS schemes require less IFFTs to generate several candidate OFDM signals compared to SLM schemes.

The conventional PTS scheme has excellent PAPR reduction performance due to the simple idea that the candidate OFDM signal with the lowest PAPR is selected for transmission among candidate OFDM signals generated by the partition and phase rotation of the original OFDM signal. However, because the conventional PTS scheme requires lots of computational complexity, various low-complexity PTS schemes have been proposed [13]–[24]. In the early times, one type of low-complexity PTS schemes [13]–[16] were proposed to use simplified searches for the optimal OFDM signal, where the signal with the lowest PAPR among many candidate OFDM signals is selected using various combinatorial optimization algorithms instead of an exhaustive search. Another low-complexity PTS scheme [17] was proposed to reduce the computational complexity

for the generation of candidate OFDM signals and to search for the transmitted OFDM signal by utilizing the structural properties of FFT and IFFT. Recently, low-complexity PTS schemes with better performance and efficiency using the artificial bee colony algorithm [18], a greedy and genetic algorithm [19], and a modified chaos clonal shuffled frog leaping algorithm [20] have been proposed. Low-complexity PTS schemes utilizing pseudo-random sequences to generate the candidate OFDM signals have also been proposed [21, 22].

The reduced-complexity PTS (RC-PTS) [23] was proposed to reduce the computational complexity by estimating the PAPRs of candidate OFDM signals based on only the selected dominant time-domain samples and then to find the candidate OFDM signal with the lowest estimated PAPR for transmission. Subsequently, improved reduced-complexity PTS (IRC-PTS) schemes [24] were proposed to reduce the computational complexity further and enhance the PAPR reduction performance of the RC-PTS. In order to achieve these efficiency and performance enhancements, the IRC-PTS uses different metrics to select the dominant time-domain samples.

1.2 Overview of Dissertation

The rest of the dissertation is organized as follows.

Chapter 2 introduces OFDM systems generally. First, OFDM and PAPR are briefly reviewed. Secondly, mathematically approximated HPA models are introduced. In addition, PAPR of OFDM signals is analyzed mathematically. Next, the various PAPR reduction schemes are reviewed. Subsequently, the conventional PTS schemes for the PAPR reduction are introduced. Finally, the previous low-complexity PTS schemes using dominant time-domain samples are explained.

In Chapter 3, new PTS schemes are proposed to reduce computational complexity using new efficient selection methods for dominant time-domain samples compared to the previous PTS schemes using dominant time-domain samples. At first, methods to

select candidate samples for dominant time-domain samples are proposed. In addition, new methods to select dominant time-domain samples based on the selected candidate samples are proposed. Lastly, low-complexity PTS schemes using the new selection method for dominant time-dominant samples are proposed in this chapter.

In Chapter 4, additional low-complexity PTS schemes are proposed to reduce computational complexity further using more efficient selection methods for dominant time-domain samples compared to RC-PTS and the PTS schemes proposed in Chapter 3. Firstly, new methods to select candidate samples adaptively for dominant time-domain samples are proposed. Also, efficient selection methods for dominant time-domain samples using the adaptively selected candidate samples are proposed. Additionally, multi-stage selection methods for dominant time-domain samples are proposed. Finally, new PTS schemes using those selection methods for dominant time-dominant samples are proposed in this chapter.

In Chapter 5, performances of the PTS schemes proposed in Chapters 3 and 4 are numerically analyzed. First, the computational complexity of the proposed PTS schemes is considered and compared to those of the previously known PTS schemes. In addition, the computational complexity of the proposed PTS schemes with specific parameters is evaluated and compared to those of the previous PTS schemes while maintaining the optimal PAPR reduction performance.

Finally, conclusions from researches of the dissertation are given in Chapter 6.

Chapter 2

PRELIMINARIES

In this chapter, several definitions and fundamental ideas are presented to explain the proposed PTS schemes. First, OFDM and PAPR are briefly reviewed and the mathematical HPA models are introduced. Next, PAPR of OFDM signals are analyzed and then the various PAPR reduction schemes are introduced. Also, the conventional PTS schemes for the PAPR reduction are explained. Finally, the dominant time-domain samples used to estimate PAPR are introduced and then the previous low-complexity PTS schemes using dominant time-domain samples are explained.

2.1 OFDM and PAPR

In this section, OFDM systems and PAPR of the employed OFDM signals are briefly reviewed. In OFDM systems, original data bits are usually modulated by phase shift keying (PSK) or quadrature amplitude modulation (QAM). A serial block of N symbols is converted to a parallel block to generate a corresponding frequency-domain input symbol vector $\mathbf{X} = [X_0, X_1, \cdots, X_{N-1}]^T$. A time-domain OFDM signal is generated by adding N input symbols modulated onto the corresponding N orthogonal sub-

carriers (sub-channels). The complex baseband OFDM signal x_t is then obtained as

$$x_t = \frac{1}{\sqrt{N}} \sum_{k=0}^{N-1} X_k e^{j2\pi k \Delta f t}, \quad 0 \le t \le NT \tag{2.1}$$

where $j = \sqrt{-1}$, Δf denotes the sub-carrier bandwidth, and NT denotes the period of the OFDM signal in which time interval of each element is T. Note that the sub-carriers of the OFDM signal satisfy the condition $\Delta f = 1/NT$ for the orthogonal relationship.

The PAPR of the original OFDM signal is defined as

$$\mathrm{PAPR} = \frac{\max\limits_{0 \le t \le NT} |x_t|^2}{E\left[|x_t|^2\right]} \tag{2.2}$$

where $E[\cdot]$ denotes the expectation. Let L denote the oversampling factor, which is an integer larger than or equal to 1. For efficient approximation of x_t and its PAPR, only LN samples of x_t, referred to as L-times oversampled OFDM signal vectors are considered. The L-times oversampled input symbol vector $\mathbf{X}_L = [X_0, X_1, \cdots, X_{LN-1}]^T$ is obtained by padding consecutive $(L-1)N$ zeros $\underbrace{[0, 0, \cdots, 0]}_{(L-1)N}^T$ to the middle or end of the original input symbol vector. The L-times oversampled input symbol vector $\mathbf{X}_L$ is transformed to L-times oversampled OFDM signal vector $\mathbf{x}_L = [x_0, x_1, \cdots, x_{LN-1}]^T$ of which an element x_n is represented as

$$x_n = \frac{1}{\sqrt{LN}} \sum_{k=0}^{LN-1} X_k e^{\frac{j2\pi kn}{LN}}, \quad 0 \le n \le LN-1. \tag{2.3}$$

It is well known that the OFDM signal vector can be interpreted as the inverse discrete Fourier transform (IDFT) of the input symbol vector. In OFDM systems, OFDM signals are generated using IFFT, which reduces computational complexity of the IDFT. Throughout the dissertation, we abuse the notations $\mathbf{X}_L$ and $\mathbf{x}_L$ as $\mathbf{X}$ and $\mathbf{x}$, respectively. The OFDM signal vector is also abused as the OFDM signal.

It is generally known that the PAPR of the original OFDM signal can be precisely estimated from not the Nyquist-rate sampled OFDM signal with $L = 1$ but the oversampled OFDM signal with $L = 4$ [25]. The PAPR of the L-times oversampled OFDM

signals is calculated as

$$\mathrm{PAPR}\left(\mathbf{x}\right) = \frac{\max\limits_{n=0}^{LN-1} |x_n|^2}{E\left[|x_n|^2\right]}. \tag{2.4}$$

In general, OFDM signals have high PAPR values, which is one of the most important problems in the OFDM systems. The serious problems are caused by OFDM signals with high PAPR through a nonlinear HPA. If OFDM signals with high PAPR pass through nonlinear band of a HPA, the output signals have distortions. Figure 2.1 represents an example of distortion caused by OFDM signals with high PAPR through a nonlinear HPA. The distortions of signals are divided into two kinds of which one is in-band distortion and the other is out-of-band radiation. The in-band distortion and the out-of-band radiation cause BER increase and adjacent channel interference respectively in communication systems.

To solve the PAPR problems in OFDM signals, various PAPR reduction schemes have been proposed. In the latter sections of this chapter, representative PAPR reduction schemes are introduced by classifying them into iterative scheme and probabilistic scheme. PAPR reduction schemes cannot only reduce PAPRs of OFDM signals but also reduce in-band distortion and out-of-band radiation to enhance communication quality effectively in OFDM systems.

2.2 High Power Amplifier Models

In this section, mathematical models are introduced to characterize nonlinear HPAs generally. If the number of sub-carrier is large enough, OFDM signals can be approximated by a complex Gaussian process by central limit theorem. Therefore, by a Gaussian process, OFDM signals may have very wide dynamic range. This characteristic of OFDM signals may cause serious distortions, which is nonlinear in a practical implementation since devices such as analog-to-digital converter (ADC), mixer, and HPA have a finite dynamic range. Especially, HPA operating in its nonlinear regions produces AM/AM and AM/PM distortions which are the amplitude and phase distortion, respectively and

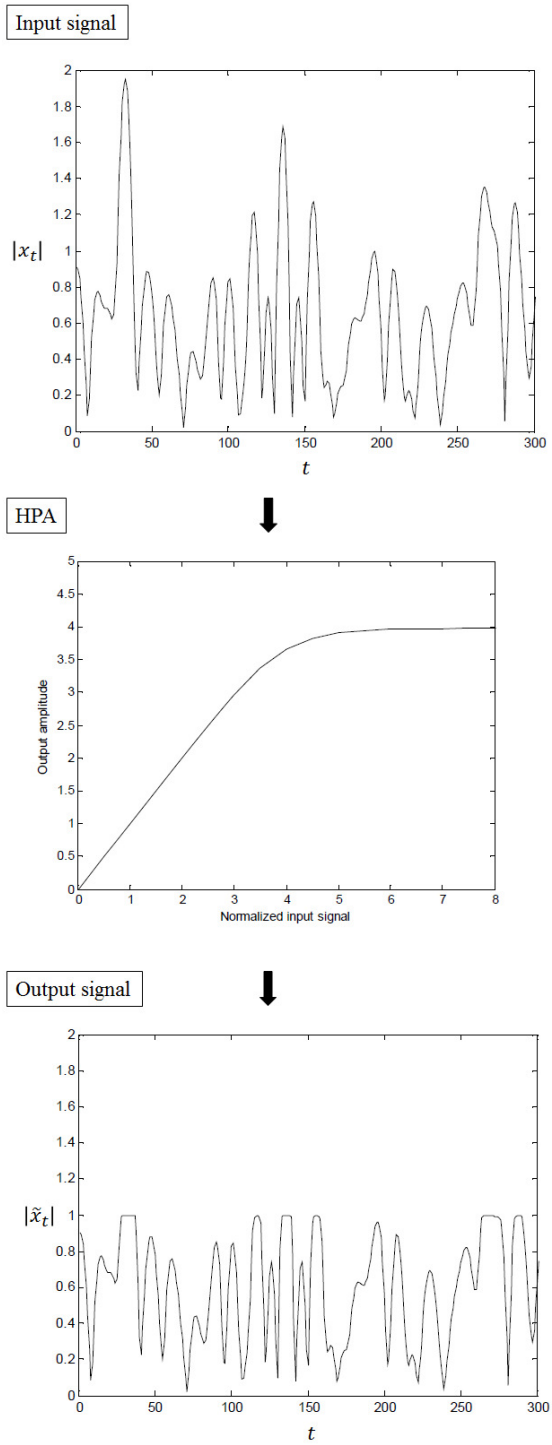

Figure 2.1: An example of distortion caused by OFDM signals with high PAPR through a nonlinear HPA.

they generate in-band distortion and out-of-band radiation of OFDM signals. Note that in-band distortion and the out-of-band radiation of signals cause BER increase and adjacent channel interference respectively in communication systems.

Since modeling nonlinear characteristics of HPA is not easy, a simplified input-output relation of nonlinear HPA for a baseband OFDM signal $x_t = |x_t|e^{\phi_{x_t}}$ is represented as

$$s_{\text{out}}(t) = G\left[|x_t|\right] e^{j\left(\phi_{x_t} + \Phi[|x_t|]\right)} \tag{2.5}$$

where the functions $G(\cdot)$ and $\Phi(\cdot)$ denote the AM/AM and AM/PM distortions, respectively. There are typically two models used for characterizing a nonlinear HPA. In the model called traveling wave tube amplifier (TWTA) [26], an input-output relation of nonlinear HPA for x_t is represented by Saleh's model as

$$G\left[|x_t|\right] = \frac{\alpha_G |x_t|}{1 + \beta_G |x_t|^2} \tag{2.6}$$

and

$$\Phi|x_t| = \frac{\alpha_\Phi |x_t|^2}{1 + \beta_\Phi |x_t|^2} \tag{2.7}$$

where the parameters α_G, β_G, α_Φ, and β_Φ determine the characteristics of TWTA.

On the other hand, the other model called solid state power amplifier (SSPA) [27] is useful for low and medium power level of nonlinear HPAs such as GaAs FET based amplifiers. In SSPA, an input-output relation for x_t is modeled as

$$G\left[|x_t|\right]] = \frac{g_0 |x_t|}{\left[1 + \left(\frac{|x_t|}{x_{\text{sat}}}\right)^2 p\right]^{\frac{1}{2p}}} \tag{2.8}$$

and $\Phi|x_t| = 0$, where g_0 denotes a small signal gain, x_{sat} denotes an input saturation level, and p determines the smoothness of the transition from the linear region to the saturation region. Note that AM/PM conversion is assumed to be very small and usually negligible to be zero.

2.3 Analysis of PAPR

In this section, PAPR of signals in OFDM systems is analyzed mathematically. In addition, BER affected by PAPR of signals in OFDM systems is also introduced analytically.

2.3.1 PAPR of OFDM Signal

An OFDM signal is sum of many independent complex signals modulated onto orthogonal sub-carriers with constant inter-carrier spacing of equal bandwidth. The PAPR of the passband OFDM signal is defined as the ratio between the maximum power and the average power of the signals as

$$\mathrm{PAPR}\left(x_{t,\mathrm{PB}}\right) = \frac{\max\limits_{0\le t<T_u} \left|x_{\mathrm{PB}}\left(t\right)\right|^2}{P_{\mathrm{av,PB}}}, \quad 0 \le t < T_u. \tag{2.9}$$

$P_{\mathrm{av,PB}}$ denotes the average power of the passband OFDM signal $x_{t,\mathrm{PB}}$ and is represented as

$$\begin{aligned} P_{\mathrm{av,PB}} &= E\left[\left|x_{t,\mathrm{PB}}\right|^2\right] \\ &= \sigma_{\mathrm{PB}}^2 \end{aligned} \tag{2.10}$$

where σ_{PB} denotes the magnitude of $x_{t,\mathrm{PB}}$.

On the other hand, the PAPR of the baseband OFDM signal is defined as

$$\mathrm{PAPR}\left(x_t\right) = \frac{\max\limits_{0\le t<T_u} \left|x_t\right|^2}{P_{\mathrm{av}}}, \quad 0 \le t < T_u \tag{2.11}$$

where P_{av} denotes the average power of the baseband OFDM signal x_t and is represented as

$$\begin{aligned} P_{\mathrm{av}} &= E\left[\left|x_t\right|^2\right] \\ &= E\left[\left|a^{\langle l\rangle}\left(t\right)\right|^2\right] \\ &= \sigma^2. \end{aligned} \tag{2.12}$$

Note that

$$\mathrm{PAPR}\left(x_{t,\mathrm{PB}}\right) \approx 2\mathrm{PAPR}\left(x_t\right). \tag{2.13}$$

The relationship in (2.13) is easily derived from

$$\max_{0\le t<T_u} \left|x_{t,\mathrm{PB}}\right|^2 \approx \max_{0\le t<T_u} \left|x_t\right|^2 \tag{2.14}$$

and

$$P_{\mathrm{av,PB}} \approx \frac{1}{2} P_{\mathrm{av}}. \tag{2.15}$$

Since σ^2 is a statistical mean, it does not vary in different OFDM blocks and the average power of x_t can be represented by the function of modulation order M in QAM modulation as

$$P\left(M\right) = \frac{M-1}{6} d_{\min}^2 \tag{2.16}$$

where $d_{\min}$ is the smallest distance between M-QAM symbols. Clearly, σ^2 is constant with the same value for all modulations by M-PSK.

In some analyses of PAPR, it is needed to define PAPR for the average power of a given OFDM signal [28] as

$$\mathrm{PAPR}_{\mathrm{G}}\left(x_t\right) = \frac{\max\limits_{0\le t<T_u} \left|x_t\right|^2}{P_{\mathrm{av,G}}}, \quad 0 \le t < T_u. \tag{2.17}$$

$P_{\mathrm{av,G}}$ is calculated as

$$\begin{aligned} P_{\mathrm{av,G}} &= \frac{1}{T_u} \int_0^{T_u} \left|x_t\right|^2 dt \\ &= \frac{1}{N} \sum_{k=0}^{N-1} \left|X_k\right|^2 \end{aligned} \tag{2.18}$$

and it is the same as σ^2 in the case of PSK modulation. In QAM modulation, $P_{\mathrm{av,G}}$ may vary according to the distribution of X_k but comes close to σ^2 as N increases. Since N is usually large enough in OFDM systems, $P_{\mathrm{av,G}}$ in case of QAM modulation is also approximately the same as σ^2.

In practical implementation of PAPR reduction scheme, PAPR for the baseband discrete OFDM signal obtained by (2.3) should be calculated as

$$\mathrm{PAPR}\left(x_n\right) = \frac{\max\limits_{0\le t<T_u} |x_n|^2}{P_{\mathrm{av}}}, \quad 0 \le n < LN. \tag{2.19}$$

Nyquist sampled discrete OFDM signals do not represent the continuous time OFDM signals exactly. Also, the PAPR of the discrete OFDM signals is usually smaller than that of the continuous OFDM signals [29, 30]. Therefore, the discrete OFDM signals should be oversampled to approximate the continuous OFDM signals. It is shown that PAPR of the oversampled discrete OFDM signals can approximate that of the continuous OFDM signals if the oversampling factor L is more than 4. The reason is an error caused by sampling and an upper bound of the error is derived in [31] as

$$\left| \max_{0\le t<T_u} |x_t| - \max_{0\le t<T_u} |x_n| \right| \le N \left[\cos^{-1}\left(\frac{\pi}{2L}\right) - 1 \right]. \tag{2.20}$$

For large N, the real and imaginary parts of the complex discrete OFDM signal x_n are approximately modeled as Gaussian random processes by central limit theorem. Also, the amplitude of x_n can be assumed to be Rayleigh distributed. Based on the above approximations, the probability that the PAPR of OFDM signal x_n with N sub-carriers is higher than a threshold λ is represented by a complementary cumulative distribution function (CCDF) as

$$\begin{aligned} \Pr\left(\mathrm{PAPR}\left(x_n\right) > \lambda\right) &= 1 - \left(\Pr\left(|x_n| \le \lambda\right)\right)^N \\ &\approx 1 - \left(1 - e^{-\lambda}\right)^N. \end{aligned} \tag{2.21}$$

Various CCDFs of PAPR distributions of OFDM signals are represented in Figures 2.2, 2.3, and 2.4. Note that QAM modulation is used for the CCDFs. Figure 2.2 shows CCDFs of PAPR distributions for OFDM signals with various signal length N. In Figure 2.2, it is shown that PAPRs of OFDM signals increase as N increases. In addition, Figure 2.3 represents CCDFs of PAPR distributions for OFDM signals with various modulation order M, respectively. From Figure 2.3, it is concluded that M does not

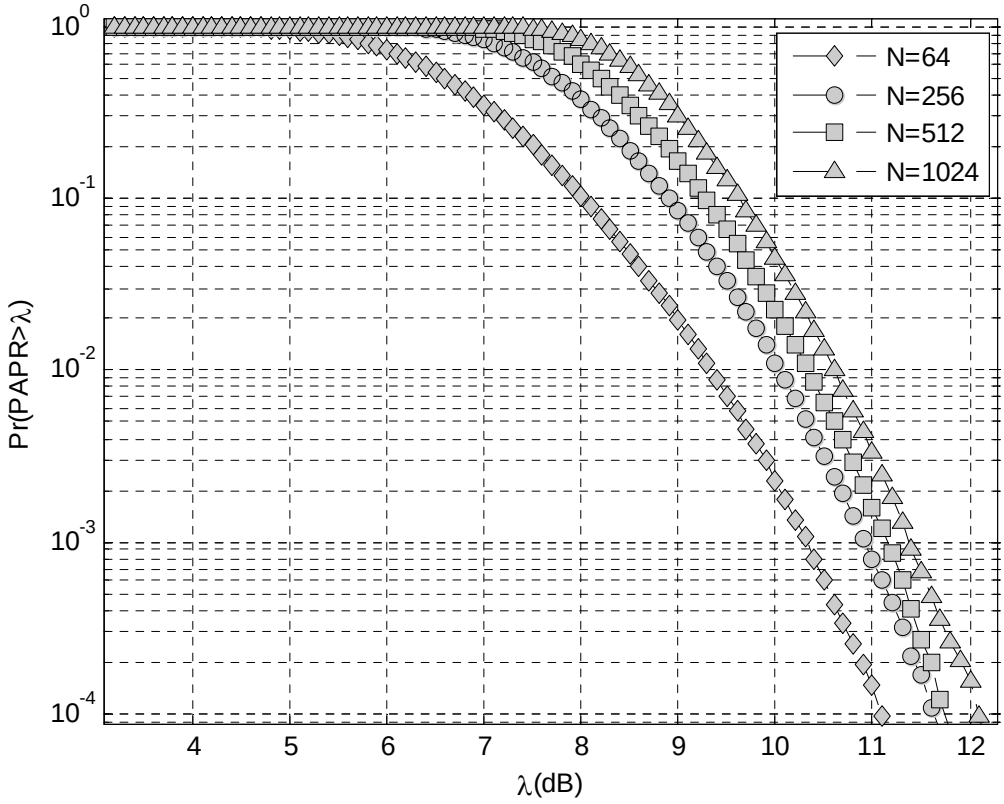

Figure 2.2: CCDFs of PAPR distributions of OFDM signals with various N for 16-QAM and $L = 1$.

affect the PAPR distribution of OFDM signals. Also, Figure 2.4 also shows the CCDFs of PAPR distributions for OFDM signals with various oversampling factor L. In Figure 2.4, it is noted that the PAPR distribution of OFDM signals with $L = 4$ is almost identical to that with $L = 16$. Note that OFDM signals with $L = 16$ can be regarded as the same as continuous OFDM signals. Therefore, it is generally known that OFDM signals with $L = 4$ approximately represents continuous OFDM signals with high accuracy.

In case that some PAPR reduction schemes are applied to the OFDM signals and then the signals are distorted, the average power σ^2 in (2.12) becomes different with

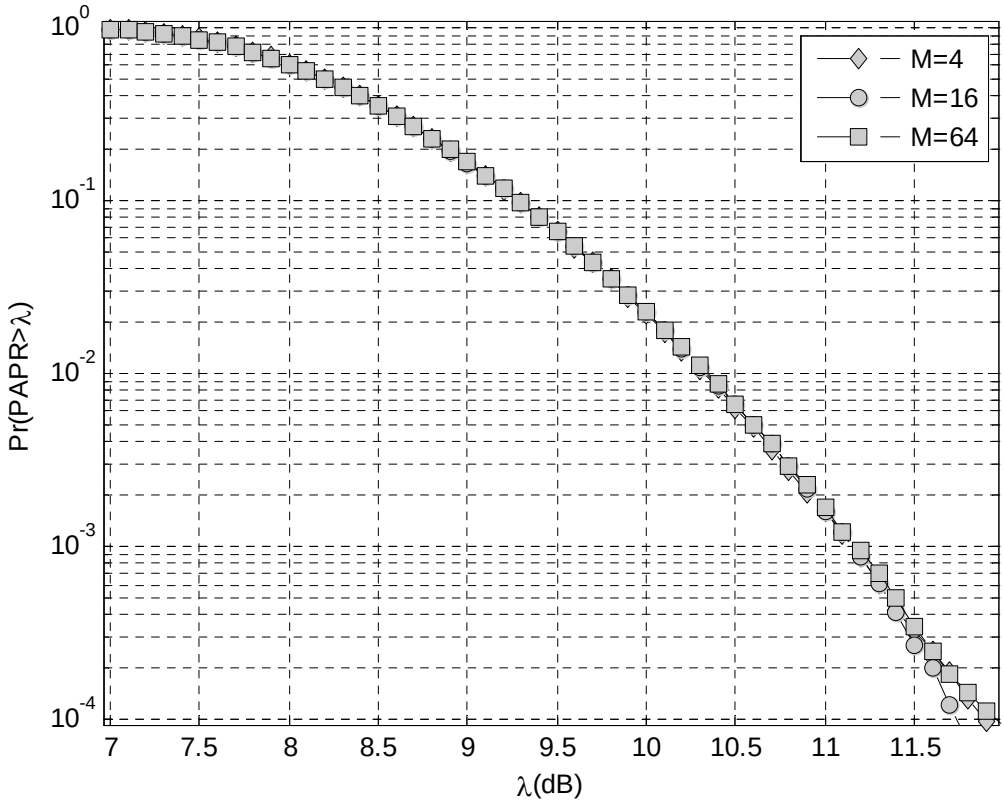

Figure 2.3: CCDFs of PAPR distributions of OFDM signals with various M for $N = 512$ and $L = 1$.

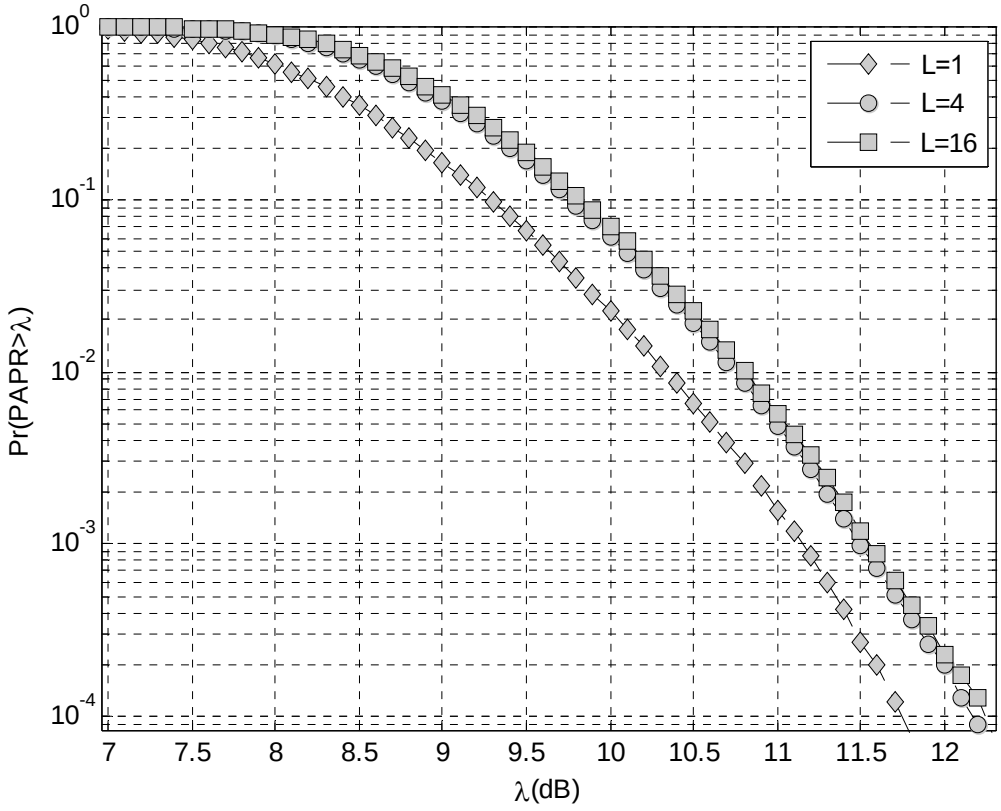

Figure 2.4: CCDFs of PAPR distributions of OFDM signals with various L for $N = 512$ and 16-QAM.

$P(M)$ in (2.16). If σ^2 becomes larger than $P(M)$, $P(M)$ is used as denominator to calculate the PAPR of OFDM signals in (2.11) for fair comparison. On the other hand, in case that σ^2 becomes smaller than $P(M)$, they can consider the shaping gain defined as

$$\gamma_{\text{SG}} = \frac{P(M)}{\sigma^2}. \tag{2.22}$$

The PAPR reduction scheme with the shaping gain γ_{SG} larger than one can improve BER performance by extending $d_{\min}$ for the same transmission power as the original OFDM symbols.

2.3.2 PAPR and BER

As mentioned in the previous section, OFDM signals may have wide dynamic range. It means that if the signals pass through HPAs with finite linear range, they may have serious nonlinear distortions. These distortions affect degradation of BER performance on received signals in OFDM systems. In order to solve this degradation problem of BER in OFDM systems, PAPR reduction of OFDM signals is indeed required and various PAPR reduction schemes have been proposed. PAPR reduction schemes can lower PAPR of OFDM signals and it matches dynamic range of OFDM signals with targeted linear range of HPAs. Thus, PAPR reduction of OFDM signals reduces the signal distortions caused in nonlinear range of HPAs and therefore enhance the BER performance.

Research in [28] explains relationship between PAPR and BER in OFDM systems. Figure 2.5 shows relationship between them of OFDM signals with QPSK ($M = 4$) modulation numerically. In this results, signal length $N = 16$ and $N = 256$ are set and a probabilistic PAPR reduction scheme as introduced in Section 2.5 is used for PAPR reduction of OFDM signals. In the probabilistic PAPR reduction scheme, U candidate signals for representing original OFDM signals are used to reduce PAPR of them. As number of candidate signals increases, PAPR reduction performance is improved but computational complexity increases. In Figure 2.5, note that “No Scaling” means a case

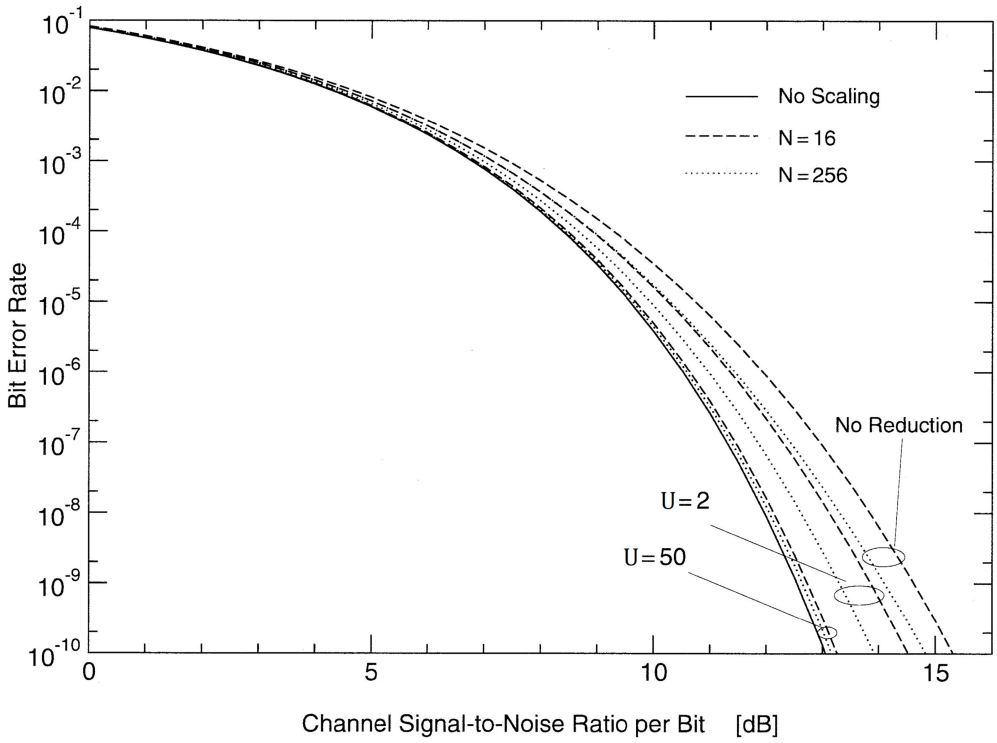

Figure 2.5: BER of uncoded OFDM signals with QPSK modulation.

in which HPAs are not used and thus no distortion is caused by passing through HPAs. Also, “No Reduction” denotes a case in which no PAPR reduction is operated. Results in Figure 2.5 show that PAPR reduction schemes can enhance BER performance of signals in OFDM systems.

2.4 Iterative PAPR Reduction Schemes

In this section, various iterative PAPR reduction schemes are reviewed. The iterative schemes directly reduce peaks of OFDM signals. Therefore, they cause in-band distortion and out-of-band radiation during peak reduction. To suppress the in-band distortion and out-of-band radiation, several iterative processes are required.

2.4.1 Clipping and Filtering

Clipping the OFDM signal is usually realized by soft envelope limiter defined as

$$\bar{x}_n = \begin{cases} x_n, & |x_n| \leq A_{th} \\ A_{th} e^{j\theta_n}, & |x_n| > A_{th} \end{cases} \tag{2.23}$$

where $x_n = |x_n| e^{j\theta_n}$ and positive value A_{th} denotes the preset target threshold level. Clipping scheme guarantees to reduce PAPR of the OFDM signal to the targeted threshold level. However, it causes in-band distortion and out-of-band radiation by distorting the OFDM signal nonlinearly. Note that the in-band distortion increases BER of the received OFDM signals and the out-of-band radiation causes interference to the signals in the neighboring channels.

To mitigate the interference in the adjacent channels, clipping and filtering (CAF) scheme was proposed [4]. The CAF scheme is the iterative scheme where the clipped signal $\bar{x}_n$ is transformed to the frequency domain symbol $\bar{X}_k$ by FFTing $\bar{x}_n$ and $\bar{X}_k$'s in out-of-band, that is, $N \leq n < LN$ are set to zero, which means the operation of out-of-band radiation removal. Since out-of-band radiation removal causes peak regrowth of the clipped OFDM signal, a clipping and filtering process is required to be iterated until PAPR of the iteratively clipped and filtered OFDM signal meets the targeted threshold level or the number of iterations reaches the predetermined maximum number.

Therefore, the CAF scheme is quite a simple method but many FFT and IFFT operations in the iterative process are needed to achieve the desired PAPR reduction performance. Note that a FFT or IFFT operation requires a lot of complex additions and multiplications. It means that the CAF have a problem of high computational complexity, which is mainly caused by many FFT and IFFT operations.

2.4.2 Tone Reservation

Tone reservation (TR) scheme reserves some tones for generating a PAPR reduction signal instead of data transmission [6]. Let $\mathcal{R} = \{i_1, i_2, \cdots, i_W\}$ denote the ordered set of the positions of the reserved tones and $\mathcal{R}^{\mathrm{c}}$ denote the complement set of $\mathcal{R}$ in $\mathcal{N} = \{0, 1, \cdots, N-1\}$ where W denotes the numbers of the reserved tones. In the TR scheme, an input OFDM symbol X_k is expressed as

$$\begin{aligned} X_k &= A_k + C_k \\ &= \begin{cases} A_k, & k \in \mathcal{R}^{\mathrm{c}} \\ C_k, & k \in \mathcal{R} \end{cases} \end{aligned} \tag{2.24}$$

where A_k denotes the data symbol with 0 in the set $\mathcal{R}$ and C_k denotes the peak reduction symbol with 0 in the set $\mathcal{R}^{\mathrm{c}}$. Figure 2.6 illustrates input OFDM symbols, which are generated by combining data symbols and peak reduction symbols in TR scheme. Let x_n, a_n, and c_n be the time-domain signals obtained by IFFTing X_k, A_k, and C_k, respectively. Since IFFT is a linear operation, the baseband discrete-time OFDM signal x_n corresponds to the summation of the data signal a_n and the PAPR reduction signal c_n, i.e., $x_n = a_n + c_n$.

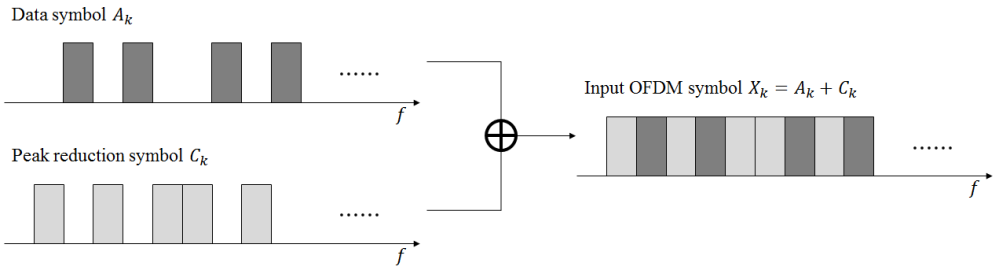

Figure 2.6: Input OFDM symbols of TR scheme.

In the TR scheme, the PAPR of the input signal vector $\mathbf{x}$ is defined as

$$\mathrm{PAPR}(\mathbf{x}) = \frac{\max\limits_{0 \le n \le N-1} |a_n + c_n|^2}{\mathrm{E}\left[|x_n|^2\right]}. \tag{2.25}$$

It should be noted that the denominator is not $\mathrm{E}\left[|x_n + c_n|^2\right]$ but $\mathrm{E}\left[|x_n|^2\right]$. The reason is that if $\mathrm{E}\left[|x_n + c_n|^2\right]$ is used as the denominator in the PAPR of the input signal vector, the PAPR can be reduced simply by increasing the average power of c_n.

Next, the generation method of peak reduction signals is introduced. Peak reduction signals are iteratively generated as follows. Let $\mathbf{p} = [p_0, p_1, \cdots, p_{N-1}]^T$ be the time-domain kernel signal vector, of which an element p_n is defined as

$$p_n = \frac{1}{\sqrt{N}} \sum_{k \in \mathcal{R}} P_k e^{\frac{j2\pi kn}{N}} \tag{2.26}$$

where $\mathbf{P} = [P_0, P_1, \cdots, P_{N-1}]^T$ denotes peak reduction tone (PRT) vector where $P_k = 0$ for $k \in \mathcal{R}^{\mathrm{c}}$. The kernel signal $\mathbf{p}$ is used to compute the PAPR reduction signal vector $\mathbf{c}$ iteratively [6]. That is, the PAPR reduction signal vector $\mathbf{c}^l$ at the lth iteration is obtained as

$$\mathbf{c}^l = \sum_{i=1}^{l} \alpha_i \mathbf{p}_{(\tau_i)} \tag{2.27}$$

where $\mathbf{p}_{(\tau_i)}$ denotes a circular shift of $\mathbf{p}$ by τ_i and α_i denotes a complex scaling factor computed according to the target threshold level γ_{th} and the maximum peak value at the ith iteration. The circular shift τ_i is determined as

$$\tau_i = \arg \max_{0 \le n \le LN-1} \left| a_n + c_n^{i-1} \right|. \tag{2.28}$$

Then, the OFDM signal in the TR scheme at the lth iteration can be represented as

$$\mathbf{x} = \mathbf{a} + \mathbf{c}^l. \tag{2.29}$$

By the shift property of the Fourier transform, it is always the case that elements of $\mathbf{Q}^{-1}\mathbf{p}_{(\tau_i)}$ and $\mathbf{C}^l = \mathbf{Q}^{-1}\mathbf{c}^l$ are zero in $\mathcal{R}^{\mathrm{c}}$, where $\mathbf{Q}^{-1}$ denotes the FFT matrix. Therefore, the iteratively generated PAPR reduction signal vector does not affect the data symbols. If the maximum number of iterations is reached or the desired peak power is obtained, iteration stops. For simplicity, it is assumed that only one maximum peak of the OFDM signal vectors is reduced in an iteration stage. Figure 2.7 shows a block diagram of TR scheme.

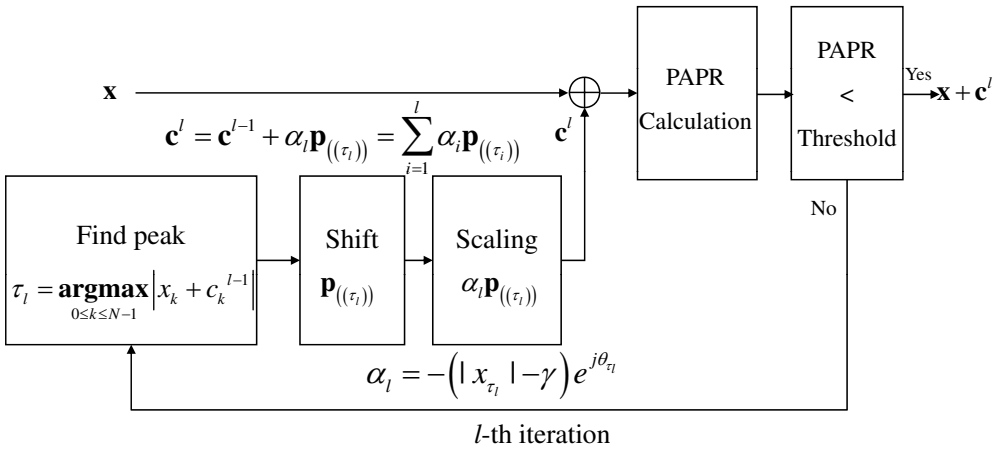

Figure 2.7: A block diagram of TR scheme.

The PAPR reduction performance of the TR scheme depends on the selection of the PRT set $\mathcal{R}$. However, this problem is known as NP-hard, because the kernel $\mathbf{p}$ must be optimized over all possible discrete sets $\mathcal{R}$. Thus, it cannot be solved for practical values of N. To solve the problem, an efficient method is proposed for selecting a near optimal PRT set [11].

As an efficient TR scheme, a multi-stage TR scheme was proposed to enhance data rate compared to previous TR schemes [12]. The multi-stage TR scheme selects one of several PRT sets adaptively according to the PAPR of the OFDM signal while the PRT set is fixed for the conventional TR scheme. In fact, the multi-stage TR scheme utilizes the conventional TR schemes in a sequential manner.

Figure 2.8 shows a two-stage TR scheme where the first TR block TR_1 is the conventional TR scheme using R_1 and γ_1 as its PRT set and threshold level, respectively, while the second TR block TR_2 uses R_2 and γ_2. In this scheme, the peak of an OFDM signal is initially reduced by TR_1 using the threshold level γ_1. After processing by TR_1, the OFDM signal is transmitted, if the PAPR of the processed OFDM signal is lower than the target PAPR threshold level γ_2. Otherwise, the OFDM signal must be processed by TR_2 for further reduction of PAPR. For the two-stage TR scheme, additional side

information of 1-bit must be transmitted to indicate which TR block is used. Assume a two-stage TR scheme where the first TR block TR_1 is the conventional TR scheme using R_1 and γ_1 as its PRT set and the target threshold level, respectively, while the second TR block TR_2 uses R_2 and γ_2.

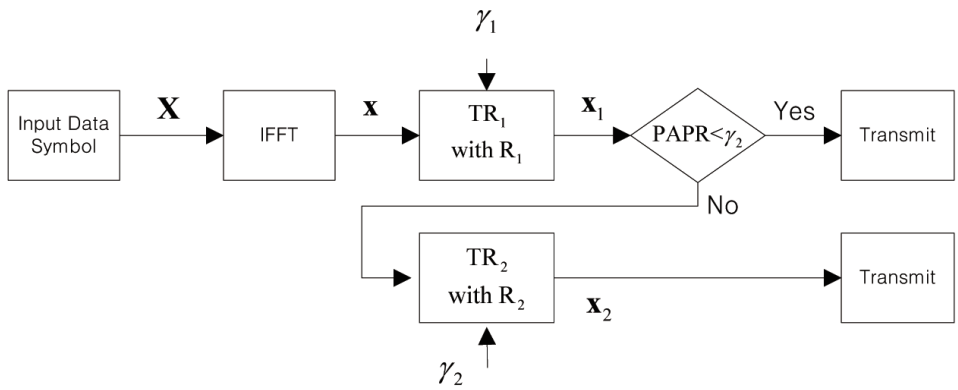

Figure 2.8: A block diagram of multi-stage TR scheme.

The two PRT sets must be designed to satisfy the condition, $R_1 \subset R_2$. The peak of an OFDM signal is initially reduced by TR_1 using the target threshold level γ_1 to generate the peak reduced OFDM signal vector $\mathbf{x}_1$. After processing by TR_1, $\mathbf{x}_1$ is transmitted, if the PAPR of the processed OFDM signal is lower than the target PAPR threshold level γ_2. Otherwise, $\mathbf{x}_1$ must be processed by TR_2 for further reduction of PAPR. For the two-stage TR scheme, additional side information of 1-bit must be transmitted to indicate which TR block was used.

The average tone reserved ratio (TRR) of the two-stage TR scheme is defined as

$$\rho_{\text{av}} = \rho_1 \Pr\left(\text{PAPR}\left(x_{1,n}\right) < \gamma_2\right) + \rho_2 \left(1 - \Pr\left(\text{PAPR}\left(x_{1,n}\right) < \gamma_2\right)\right) \tag{2.30}$$

where ρ_1 and ρ_2 denote the TRR values of TR_1 and TR_2, respectively, and $\text{PAPR}(x_{1,n})$ denotes the PAPR of x_1 after TR_1 is applied.

Since $\rho_2 > \rho_1$, to minimize ρ_{av}, it is desirable to select the threshold level γ_1 such that $\Pr(\text{PAPR}(x_{1,n}) < \gamma_2)$ is quite high (≥ 0.9). Then, the two-stage TR scheme can

reduce the PAPR level of OFDM signals below the target threshold level γ_2 while achieving an average TRR close to ρ_1. In other words, it is possible to obtain the desired peak power reduction with the smaller number of iterations than that of the conventional TR for the same data rate and as a consequence, the proposed scheme can reduce the computational complexity considerably.

2.4.3 Active Constellation Extension

Active constellation extension (ACE) scheme reduces the amplitude of peak signals by extending sub-carriers located at exterior constellations to outer region to keep minimum distance between symbols [7]. It is aimed to reduce PAPR by clipping without BER performance degradation and out-of-band radiation. However, there are some transmit power increase and additional complexity with this scheme.

Let $\mathbf{C}_{\text{PRD}} = \{C_0, C_1, ..., C_{LN-1}\}$ be the set of peak reduction data in frequency domain and $\mathcal{C}_{\text{ext}}$ represent allowable space of peak reduction data satisfying ACE constraint. Then ACE minmax problem can be formulated as

$$\min_{\mathbf{C} \in \mathcal{C}_{\text{ext}}} \max |\hat{x}_n| \tag{2.31}$$

where

$$\begin{aligned} \hat{x}_n &= x_n + c_n \\ &= \frac{1}{\sqrt{N}} \sum_{k=0}^{LN-1} (X_k + C_k)\, e^{\frac{j2\pi nk}{LN}}. \end{aligned} \tag{2.32}$$

For example, if we use soft envelope limiter in (2.23) to reduce signals of which amplitude is larger than A_{th}, $\mathbf{C}_{\text{PRD}}$ is the set of data given by IFFTing the clipping noise c_n and it is usually non-zero value for $C_k, 0 \leq k \leq LN-1$. After applying ACE constraint, the peak reduction data located at outward of exterior constellation are projected to the position where the resulting OFDM symbols keep their minimum distance and the others including peak reduction data in out-of-band are set to zero. Consequently, $\mathbf{C}_{\text{PRD}}$ becomes the subset of $\mathcal{C}_{\text{ext}}$.

ACE uses non-bijective constellations to reduce the PAPR by appropriately encoding the data symbols. The idea is easily explained in the case of OFDM systems with QPSK modulation in each sub-carrier. For an individual sub-carrier, there are four possible constellation points, which lie in each quadrant in the complex plane and are equidistant from the real and imaginary axes. Assuming that channel is affected by additive white Gaussian noise (AWGN), the maximum-likelihood (ML) decision regions are the four quadrants bounded by the axes and thus a received data symbol is assigned according to the quadrant in which the symbol is observed. Since only one of the four constellation points can be transmitted at a time, errors occur when noise translates the received symbol into one of the other three quadrants. Any point farther from the decision boundaries than the nominal constellation point (in the proper quadrant) will offer increased margin, which guarantees a lower error rate. Therefore, in ACE, modification of constellation points is allowed within the quarter-plane outside of the nominal constellation point with no degradation of BER performance.

This principle of ACE is illustrated in Figure 2.9 where Figures 2.9(a) and (b) show modifications of constellation points in QPSK ($M = 4$) and 16-QAM modulation, respectively. In Figure 2.9(a), the shaded region represents the region of increased margin for the data symbol in the four quadrants. In OFDM systems with ACE, the effect of moving into the shaded region is to add additional symbols in the particular sub-carriers to the original OFDM symbols. if adjusted intelligently, a combination of these additional symbols can be used to partially cancel peaks of original time-domain OFDM signals. In Figure 2.9(b), the shaded region represents corner-point extension regions. Also, the dotted and arrowed lines represent the extension paths for side points. The ACE idea can be applied to other PSK and QAM constellations as well, since symbol points on the outer boundaries of the constellations have room for increased margin without degrading BER for other symbols. In the case of BPSK, alteration of the constellation point within the half-plane of equal or greater distance from the decision boundary is acceptable. For square QAM constellations, interior points cannot

be moved, side points can be extended only outward in one direction, and corner points have the flexibility to be translated outward in two directions.

Some practical methods to solve this optimization problem are proposed in [7]. Projection onto convex set (POCS) method achieves optimal solution but converges very slowly. Smart gradient project (SGP) method which uses gradient step size to improve convergence speed is sub-optimal solution but faster than POCS.

Since ACE method uses degree of freedom of data located at exterior constellation to reduce PAPR, it does not need any additional process at receiver which means that it can be applied to the existing systems with minor modification at transmitter. Moreover, there is no loss in data rate because it does not need any side information or extra tones. Drawbacks of ACE are the increased signal power and the large computational complexity due to iterative process. If it is possible to reduce the amount of peak regrowth due to ACE constraint, ACE can achieve the same PAPR reduction performance as that of the conventional ACE with the smaller number of iterations. One of the possible scheme is to use peak cancelling instead of clipping. There will be no peak regrowth if PRT set is constructed such that the peak reduction data after peak cancelling are in a subset of $\mathcal{C}_{\text{ext}}$. However, it is impossible to find PRT set satisfying this condition before peak cancelling. Instead, it can be suboptimal to allow PRT set to have valid value only at the same indices as symbols located at exterior constellation.

2.5 Probabilistic PAPR Reduction Scheme: Selective Mapping

In this and the next section, probabilistic PAPR reduction schemes called selective mapping (SLM) and partial transmit sequence (PTS) are introduced, respectively. The probabilistic schemes generate multiple candidate OFDM signal vectors to represent a OFDM signal vector. And then a candidate OFDM signal vector with the minimum PAPR is selected among all the candidate OFDM signal vectors and transmitted as an

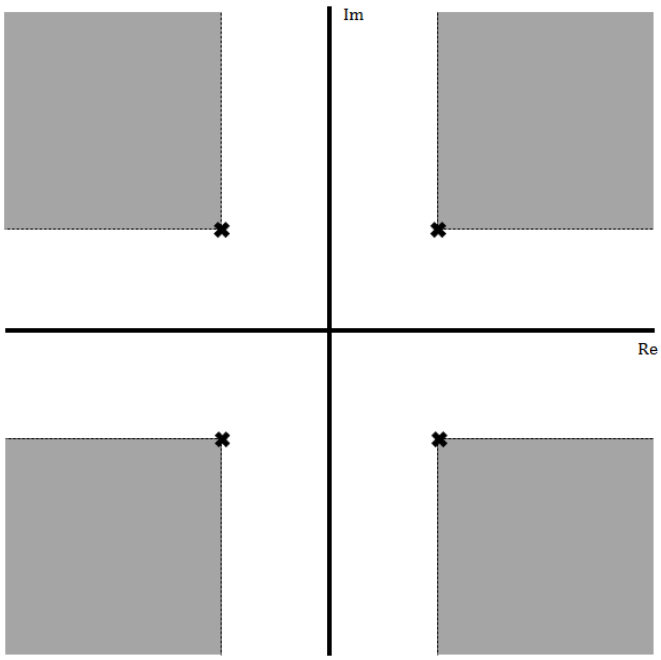

(a) QPSK modulation

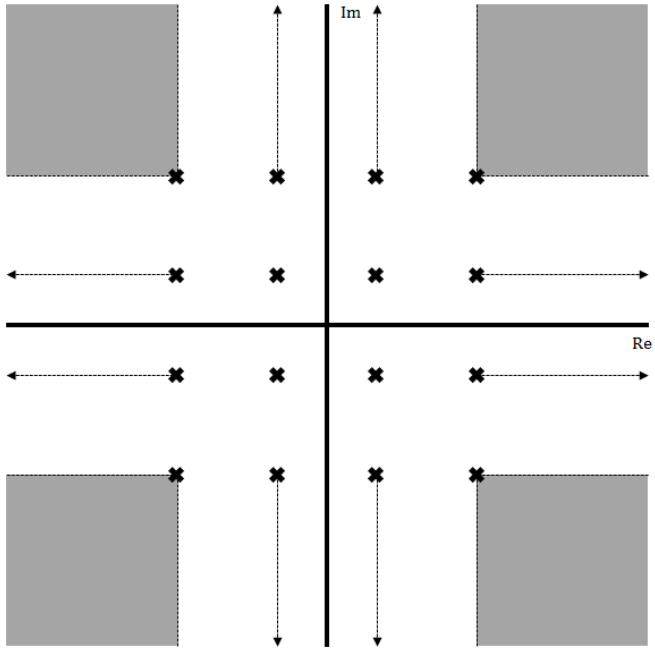

(b) 16-QAM modulation

Figure 2.9: Modified constellations of modulations in ACE scheme.

OFDM signal vector. In the probabilistic schemes, high-complexity computation is required to process the candidate OFDM signal vectors.

In the SLM scheme [9], U candidate symbol vectors $\mathbf{X}^{(u)} = \left[X_0^{(u)}, X_1^{(u)}, \cdots, X_{N-1}^{(u)}\right]^T$, $1 \leq u \leq U$ are generated via component-wise vector multiplication of the input symbol vector $\mathbf{X}$ and U phase rotation vectors $\mathbf{P}^{(u)} = \left[P_0^{(u)}, P_1^{(u)}, \cdots, P_{N-1}^{(u)}\right]^T$. The notation $\mathbf{X}^{(u)} = \mathbf{X} \otimes \mathbf{P}^{(u)}$ denotes component-wise multiplication of $\mathbf{X}$ and $\mathbf{P}^{(u)}$, i.e., $X_k^{(u)} = X_k P_k^{(u)}, 0 \leq k \leq N-1$.

The phase rotation vector $\mathbf{P}^{(u)}$ is generated by using the unit-magnitude complex number, that is, $P_k^{(u)} = e^{j\phi_k^u}$, where $\phi_k^u \in [0, 2\pi)$. In general, binary or quaternary elements are used for $P_k^{(u)}$, that is, $\{\pm 1\}$ or $\{\pm 1, \pm j\}$.

IFFT operation is performed for each of U candidate symbol vectors to generate U candidate OFDM signal vectors as

$$\begin{aligned} \mathbf{x}^{(u)} &= \mathbf{Q}^H \mathbf{X}^{(u)} \\ &= \mathbf{Q}^H \left(\mathbf{X} \otimes \mathbf{P}^{(u)}\right), \quad 1 \leq u \leq U. \end{aligned} \tag{2.33}$$

Then, the OFDM signal vector with the minimum PAPR among U candidate OFDM signal vectors is selected and transmitted. The index u_{opt} of the transmitted candidate OFDM signal vector is obtained by

$$u_{\text{opt}} = \arg \min_{1 \leq u \leq U} \left(\max_{0 \leq n \leq N-1} |x_{u,n}| \right). \tag{2.34}$$

Therefore, $\mathbf{x}^{(u_{\text{opt}})}$ is selected and then transmitted as the OFDM signal vector. Figure 2.10 represents process of the conventional SLM scheme. Clearly, as U increases, PAPR reduction become large while the computational complexity becomes too high, mainly due to U IFFTs. it should be noted that there is a saturation effect, that is, the additional PAPR reduction gain decreases as U increases.

In order to recover the original input symbol vector in the receiver, the transmitter must send the side information about the index u. Note that this side information causes a slight increase in redundancy, which means date rate loss. Since the index information is important, it must be encoded for error detection and correction. If the code rate is

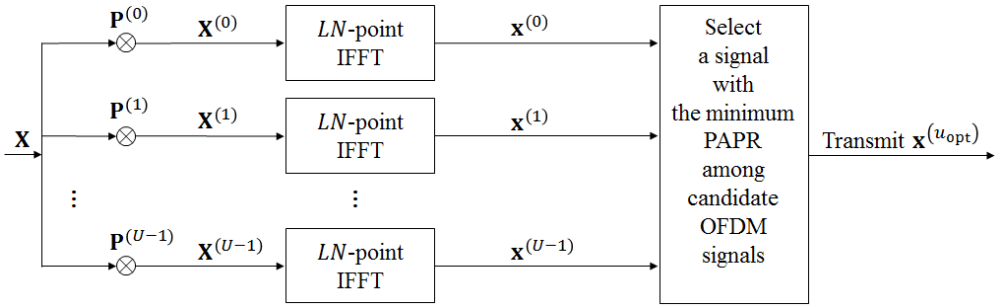

Figure 2.10: A block diagram of the conventional SLM scheme.

R and the SLM scheme using U phase rotation vectors is concerned, $\lceil \log_M(U/R) \rceil$ symbols must be transmitted where $\lceil d \rceil$ denotes the smallest integer greater than or equal to d.

In order to achieve a large PAPR reduction in the conventional SLM scheme, it has to generate a sufficiently large number of candidate OFDM signal vectors, which cause a high computational complexity because IFFT must be performed to generate each candidate OFDM signal vector. Therefore, it is desirable to reduce the number of IFFTs and avoid degradation of the PAPR reduction performance.

A new SLM scheme with low computational complexity is proposed in [32]. This is a method for applying the SLM scheme to the intermediate stage of IFFT rather than the first stage as in the previous subsection. In this scheme, the N point IFFT based on decimation-in-time algorithm is partitioned into two parts, i.e., the first l stages and the remaining $n - l$ stages. To make candidate OFDM signal vectors, it multiplies the different U phase rotation vectors, $\mathbf{P}^{(u)}, 1 \leq u \leq U$, using the signal in the intermediate lth stage of IFFT. Based on the proposed SLM scheme, the computational complexity is reduced compared to the conventional SLM scheme, because it uses a common IFFT upto l stages and then the SLM scheme is applied to the intermediate stage IFFTed signals.

Since the proposed SLM scheme is performed using a stage-by-stage IFFT approach,

its computational complexity can be reduced compared to the common IFFT operation $\mathbf{Q}_0^{l-1} = \mathbf{T}_{l-1}\mathbf{T}_{l-1}\cdots\mathbf{T}_0$. The output signal corresponding to the phase rotation vector in the proposed SLM scheme $\tilde{\mathbf{x}}$ can be expressed as

$$\tilde{\mathbf{x}} = \mathbf{T}_n\cdots\mathbf{T}_{k+1}\tilde{\mathbf{P}}\mathbf{T}_k\cdots\mathbf{T}_1\mathbf{A} \tag{2.35}$$

where $\tilde{\mathbf{P}}$ is a $2^{n-l} \times 2^{n-l}$ diagonal block matrix, i.e., each $2^l \times 2^l$ subblock of $\tilde{\mathbf{P}}$ is either $\pm\mathbf{I}_{2^l}$. Here, $\mathbf{I}_{2^l}$ is the $2^l \times 2^l$ identity matrix.

When the number of sub-carriers is $N = 2^n$, the numbers of complex multiplications n_{mul} and complex additions n_{add} of the conventional SLM scheme are given as $n_{\text{mul}} = 2^{n-1}nU$ and $n_{\text{add}} = 2^n nU$, respectively, where U denotes the total number of phase rotation vectors. If the phase rotation vectors are multiplied after the lth stage of IFFT, the numbers of complex computations of the proposed SLM scheme are given as $n_{\text{mul}} = 2^{n-1}n + 2^{n-1}(n-l)(U-1)$ and $n_{\text{add}} = 2^n n + 2^n(n-l)(U-1)$.

The proposed SLM scheme has almost the same PAPR reduction performance as that of the conventional SLM scheme for $n - l = 5$ and 16-QAM constellation. In the case of $n - l = 5$, the proposed scheme reduces the computational complexity by $41\sim51\%$ as U increases from 4 to 16.

The modified SLM scheme [33] generates some of candidate OFDM signal vectors using the other ones in the time-domain. Let $\mathbf{x}^{(i)}$ and $\mathbf{x}^{(k)}$ be the candidate OFDM signal vectors, generated by the conventional SLM scheme as in (2.33). Based on linear property of the Fourier transform, the linear combination of these two vectors can be given as

$$\begin{aligned}\mathbf{x}^{(i,k)} &= c_i\mathbf{x}^{(i)} + c_k\mathbf{x}^{(k)} \\ &= c_i\mathbf{Q}\left(\mathbf{X}\otimes\mathbf{P}^{(i)}\right) + c_k\mathbf{Q}\left(\mathbf{X}\otimes\mathbf{P}^{(k)}\right) \\ &= \mathbf{Q}\left(\mathbf{X}\otimes\left(c_i\mathbf{P}^{(i)} + c_k\mathbf{P}^{(k)}\right)\right)\end{aligned} \tag{2.36}$$

where c_i and c_k are complex numbers. If each element of the vector $c_i\mathbf{P}^{(i)} + c_k\mathbf{P}^{(k)}$ in (2.36) has a unit magnitude, $c_i\mathbf{P}^{(i)} + c_k\mathbf{P}^{(k)}$ can also be used as a phase rotation

vector for the SLM scheme and $\mathbf{x}^{(i,k)}$ can be considered as the corresponding candidate OFDM signal vector. Therefore, if candidate OFDM signal vectors $\mathbf{x}^i$ and $\mathbf{x}^k$ are prepared, another candidate OFDM signal vector $\mathbf{x}^{(i,k)}$ can be obtained, which avoids the need for IFFT. Note that the phase rotation vector $c_i\mathbf{P}^{(i)} + c_k\mathbf{P}^{(k)}$ is not statistically independent of $\mathbf{P}^{(i)}$ and $\mathbf{P}^{(k)}$. The modified SLM scheme has the method, which make each element of $c_i\mathbf{P}^{(i)} + c_k\mathbf{P}^{(k)}$ a unit magnitude, in the condition that each element of the phase rotation vectors $\mathbf{P}^{(i)}$ and $\mathbf{P}^{(k)}$ has a unit magnitude. Clearly, the elements of the vector $c_i\mathbf{P}^{(i)} + c_k\mathbf{P}^{(k)}$ have a unit magnitude if the following conditions are satisfied:

1) Each element of $\mathbf{P}^i$ and $\mathbf{P}^k$ has a value in $\{+1, -1\}$;

2) $c_i = \pm 1/\sqrt{2}$ and $c_k = \pm j/\sqrt{2}$.

Since the two candidate OFDM signal vectors generated from the phase rotation vectors $\pm(c_i\mathbf{P}^{(i)} + c_k\mathbf{P}^{(k)})$ have the same PAPR, the modified SLM scheme consider the case of $c_i = 1/\sqrt{2}$ and $c_k = \pm j/\sqrt{2}$. Since $|c_i|^2 = |c_k|^2 = 1/2$, the average power of $\mathbf{a}^{i,k}$ is equal to half the sum of the average power of $\mathbf{a}^{(i)}$ and $\mathbf{a}^{(k)}$. Using U binary phase rotation vectors, $2\binom{U}{2}$ additional phase rotation vectors are obtained, where $\binom{U}{2} = U(U-1)/2$. Thus, the total U^2 phase rotation vectors are obtained as $\{\mathbf{P}^{(1)}, \mathbf{P}^{(2)}, \cdots, \mathbf{P}^{(u)}, \frac{1}{\sqrt{2}}\left(\mathbf{P}^{(1)} \pm j\mathbf{P}^{(2)}\right), \frac{1}{\sqrt{2}}\left(\mathbf{P}^{(1)} \pm j\mathbf{P}^{(3)}\right), \cdots, \frac{1}{\sqrt{2}}\left(\mathbf{P}^{(U-1)} \pm j\mathbf{P}^{(u)}\right)\}$.

By combining each pair among U candidate OFDM signal vectors $\mathbf{x}^{(u)}$ obtained by using U binary phase rotation vectors as above, a set $\mathcal{S}$ of U^2 candidate OFDM signal vectors are generated as

$$\begin{aligned}\mathcal{S} &= \{\mathbf{x}^{(u)} | 1 \le u \le U^2\} \\ &= \{\mathbf{x}^{(u)} | 1 \le u \le U\} \cup \left\{ \frac{1}{\sqrt{2}}\left(\mathbf{x}^{(i)} + j\mathbf{x}^{(k)}\right), \frac{1}{\sqrt{2}}\left(\mathbf{x}^{(i)} - j\mathbf{x}^{(k)}\right) | 1 \le i < k \le U \right\}\end{aligned} \tag{2.37}$$

where only U IFFTs and the additional summations of $(U^2 - U)$ pairs of OFDM signal vectors are needed. However, the computational complexity for the summations of OFDM signal vectors is negligible compared with that of IFFT.

The modified SLM scheme with U binary phase rotation vectors can be compared with the conventional SLM scheme with U^2 binary phase rotation vectors. These two schemes show a similar PAPR reduction performance for a small U. However, as U increases, the PAPR reduction performance of the modified scheme becomes worse than that of the conventional SLM scheme with U^2 binary phase rotation vectors, because U^2 phase rotation vectors of the modified scheme are statistically correlated.

2.6 Conventional PTS Scheme

In the conventional PTS scheme [10], an oversampled input symbol vector $\mathbf{X}$ is partitioned into V disjoint sub-blocks $\mathbf{X}_v = [X_{v,0}, X_{v,1}, \cdots, X_{v,LN-1}]^T, 0 \leq v \leq V-1$, satisfying the condition such that

$$\mathbf{X} = \sum_{v=0}^{V-1} \mathbf{X}_v. \tag{2.38}$$

By applying IFFT to each sub-block, the sub-signal vectors $\mathbf{x}_v = [x_{v,0}, x_{v,1}, \cdots, x_{v,LN-1}]^T$, $0 \leq v \leq V-1$ are generated. In order to generate the candidate OFDM signals, each sub-signal vector is multiplied by the phase rotating factor $b_v = e^{j\phi_v}$, where $\phi_v \in [0, 2\pi)$ for $v = 0, 1, \cdots, V-1$. The phase rotating factor is usually an element of the finite set given as $b_v \in \{e^{j2\pi l/W} \mid l = 0, 1, \cdots, W-1\}$, where W is the alphabet size of the phase rotating factors. The phase rotating vectors which generate the candidate OFDM signals are represented by $\mathbf{b}^{(u)} = \left[b_0^{(u)}, b_1^{(u)}, \cdots, b_{V-1}^{(u)}\right]$, $u = 0, 1, \cdots, U-1$, where U denotes the number of candidate OFDM signals to be generated. With the u-th phase rotating vector, the u-th candidate OFDM signal $\mathbf{x}^{(u)}$ is generated as

$$\begin{aligned} \mathbf{x}^{(u)} &= \left[x_0^{(u)}, x_1^{(u)}, \cdots, x_{LN-1}^{(u)}\right]^T \\ &= \sum_{v=0}^{V-1} b_v^{(u)} \mathbf{x}_v, \quad u = 0, 1, \cdots, U-1. \end{aligned} \tag{2.39}$$

Because all of the first phase rotating factors $b_v^{(0)}, 0 \leq v \leq V-1$ are usually set to one, $U = W^{V-1}$ candidate OFDM signals are generated in the conventional PTS scheme. Finally, the optimal OFDM signal $\mathbf{x}^{(u_{\text{opt}})}$ with the minimum PAPR value among U candidate OFDM signals is selected for the transmission, where u_{opt} denotes the index of the optimal candidate OFDM signal, that is,

$$u_{\text{opt}} = \arg \min_{u=0}^{U-1} \text{PAPR}(\mathbf{x}^{(u)}). \tag{2.40}$$

The block diagram of the conventional PTS scheme is given in Figure 2.11.

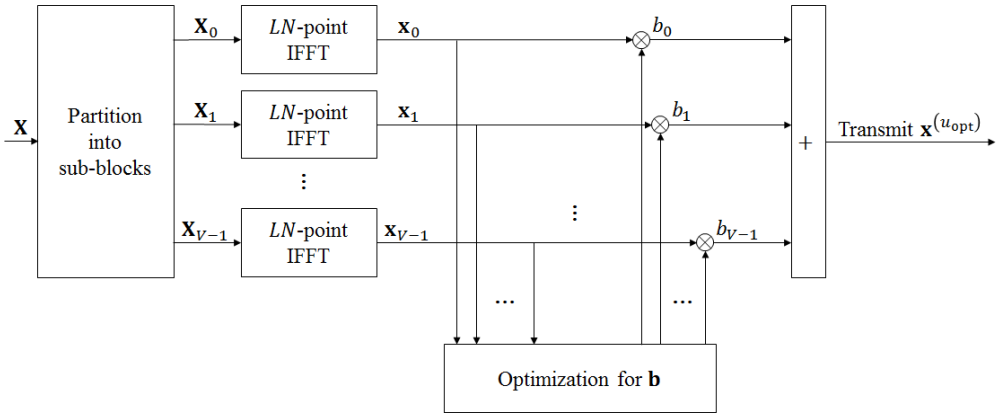

Figure 2.11: A block diagram of the conventional PTS scheme.

Although the conventional PTS scheme can achieve a considerable PAPR reduction with a simple method, there are several disadvantages. High computational complexity is the main disadvantage of the conventional PTS scheme, where most of the computational complexity comes from the generation and PAPR calculation of U candidate OFDM signals. In the following section, recently proposed low-complexity PTS schemes [23, 24] are introduced; these mainly reduce the computational complexity required for the calculation of the PAPR of the candidate OFDM signals after IFFTs. These low-complexity PTS schemes have the same idea that only a few dominant time-domain samples of candidate OFDM signals are used for the PAPR calculation instead of all of the time-domain samples. They reduce the computational complexity

considerably while maintaining identical PAPR reduction performance compared to those of the conventional PTS scheme.

2.7 Low-Complexity PTS Schemes Using Dominant Time-Domain Samples

In this section, previously proposed low-complexity PTS schemes [23, 24] are introduced. These low-complexity PTS schemes reduce computational complexity compared to the conventional PTS scheme while maintaining high PAPR reduction performance. At first, dominant time-domain samples to reduce computational complexity of PTS schemes are introduced. Then, several low-complexity PTS schemes using dominant time-domain samples are reviewed.

2.7.1 Dominant Time-Domain Samples

The conventional PTS scheme has the optimal PAPR reduction performance but its computational complexity is too high for it to be used for practical implementation in OFDM systems. One of major parts in its high computational complexity is PAPR computation of candidate OFDM signal vectors. To compute PAPRs of all candidate OFDM signal vectors, a lot of complex multiplications are required. The other major parts of computation in the conventional PTS scheme is generation of candidate OFDM signal vectors. For generation of $U = V^{W-1}$ candidate OFDM signal vectors, V IFFT operations are required to generate V sub-block vectors. Note that IFFT operations requires considerable computation of complex multiplications and additions.

Table 2.1 shows numbers of complex multiplication representing computational complexity at the two major stages in the conventional PTS scheme for general parameters N, L, V, W, and U, which denotes OFDM signal vector length, oversampling factor, number of sub-block vectors, alphabet size of phase rotating factors, and number of candidate OFDM signal vectors, respectively. Note that V, W, and U have

relationship that $U = W^{V-1}$.

Table 2.1: General computational complexity of two major stages in the conventional PTS scheme

Stages	Generation of candidate signals (including IFFTs)	Selection of OFDM signal (without IFFTs)
Number of complex multiplications	$\frac{LNV}{2} \log_2 LN$	$LNU = LNV^{W-1}$

In addition, Table 2.2 shows numbers of complex multiplication representing numerical computational complexity at the two major stages in the conventional PTS scheme for several specific parameters. Note that as V increases, relative computational complexity required for selection of OFDM signal increases and is higher that that required for generation of candidate OFDM signal. Assuming that other parameters are fixed, high V means high U, which enhances PAPR reduction performance but increases computational complexity. Therefore, in order to reduce computational complexity while maintaining high performance of PAPR reduction, it is important to lower computational complexity for selection of OFDM signal.

Recently proposed low-complexity PTS schemes [23, 24] mainly reduce the computational complexity required for the selection of OFDM signals. These PTS schemes have similar property that partial time-domain samples of candidate OFDM signals are used to estimate their PAPRs instead of all the time-domain samples. The small number of selected time-domain samples are referred to as dominant time-domain samples. If only the dominant time-domain sample are used to estimate PAPRs of candidate OFDM signals instead of calculating PAPRs of all the time-domain samples, the computational complexity for selection of transmitted OFDM signals is reduced considerably and therefore those in previous PTS schemes are reduced. Figure 2.12 illustrates dominant

Table 2.2: Computational complexity of two major stages in the conventional PTS scheme for specific parameters

(a) $W = 2$

Parameters		Number of complex multiplications	
N	V	Generation of candidate signals (including IFFTs)	Selection of OFDM signal (without IFFTs)
256	4	20480 (71.43%)	8192 (28.57%)
256	6	30720 (48.39%)	32768 (51.61%)
256	8	40960 (23.81%)	131072 (76.19%)
1024	4	98304 (75.00%)	32768 (25.00%)
1024	6	147456 (52.94%)	131072 (47.54%)
1024	8	196608 (27.27%)	524288 (72.73%)

(b) $W = 4$

Parameters		Number of complex multiplications	
N	V	Generation of candidate signals (including IFFTs)	Selection of OFDM signal (without IFFTs)
256	4	20480 (71.43%)	8192 (28.57%)
256	6	30720 (48.39%)	32768 (51.61%)
256	8	40960 (23.81%)	131072 (76.19%)
1024	4	98304 (75.00%)	32768 (25.00%)
1024	6	147456 (52.94%)	131072 (47.54%)
1024	8	196608 (27.27%)	524288 (72.73%)

time-domain samples used to estimate PAPRs of candidate OFDM signals in PTS schemes.

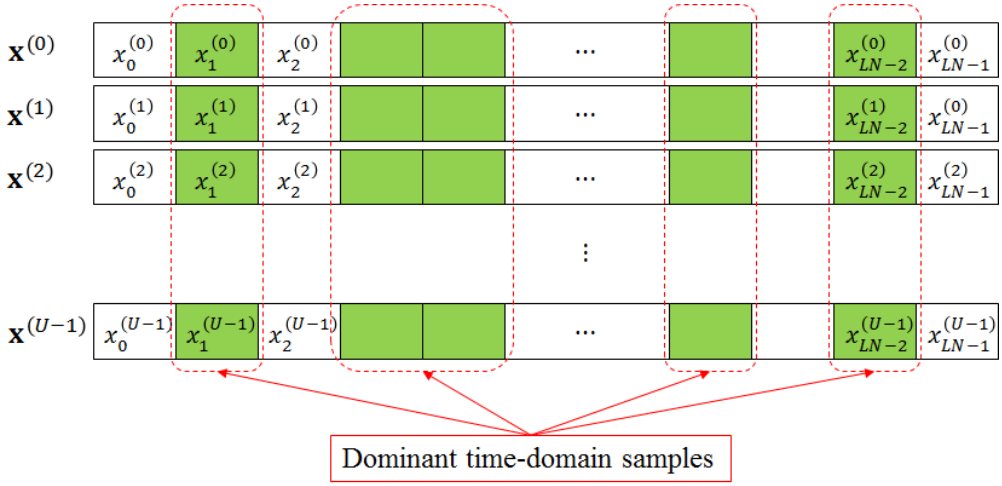

Figure 2.12: Dominant time-domain samples used in low-complexity PTS schemes.

2.7.2 Low-Complexity PTS Schemes Using Dominant Time-Domain Samples

The RC-PTS [23] is the first low-complexity PTS scheme, which utilizes only a few time-domain samples, referred to as dominant time-domain samples to estimate the peak power and the corresponding PAPR of each candidate OFDM signal. In the RC-PTS, the dominant time-domain samples are selected using a metric Q_n given by

$$Q_n = \sum_{v=0}^{V-1} |x_{v,n}|^2. \tag{2.41}$$

For an index n, if Q_n is larger than or equal to a preset threshold γ_Q, the time-domain sample x_n is selected as the dominant time-domain sample. The index set of the dominant time-domain samples is denoted as

$$\mathbf{S}_Q(\gamma_Q) = \{n \mid Q_n \geq \gamma_Q, \quad 0 \leq n \leq LN-1\}. \tag{2.42}$$

Among all of the time-domain samples, only the dominant time-domain samples with indices in $\mathbf{S}_Q(\gamma_Q)$ are used to estimate the PAPR of each candidate OFDM signal. Then, in the RC-PTS, the OFDM signal $\mathbf{x}^{(u_{\text{opt}})}$ selected for transmission is the candidate OFDM signal with the index u_{opt}, which is given as

$$u_{\text{opt}} = \arg \min_{u=0}^{U-1} \max_{n \in \mathbf{S}_Q(\gamma_Q)} \left| \sum_{v=0}^{V-1} b_v^{(u)} x_{v,n} \right|^2 . \tag{2.43}$$

Although the RC-PTS utilizes the same U candidate OFDM signals, the computational complexity for calculating the PAPR of each candidate OFDM signal is much less than that of the conventional PTS scheme and previous PTS schemes, which do not utilize dominant time-domain samples. Therefore, it is clear that the RC-PTS significantly reduces the computational complexity compared to the conventional PTS scheme.

After the RC-PTS, the IRC-PTS [24] was proposed to reduce computational complexity further compared to the conventional PTS schemes and the RC-PTS. Although the IRC-PTS uses dominant time-domain samples in a manner similar to the RC-PTS, it uses more efficient selection methods for dominant time-domain samples. In the IRC-PTS, the dominant time-domain samples are selected using metrics Y_n and A_n given by

$$Y_n = \sum_{v=0}^{V-1} |x_{v,n}| \tag{2.44}$$

and

$$A_n = \left| \sum_{v=0}^{V-1} \left(|\text{Re}\{x_{v,n}\}| + j \, |\text{Im}\{x_{v,n}\}| \right) \right| . \tag{2.45}$$

respectively. Similar to the RC-PTS, IRC-PTS reduces the computational complexity to calculate the PAPR of each candidate OFDM signal compared to the conventional PTS scheme and previous PTS schemes not utilizing dominant time-domain samples. Moreover, the computational complexity of the IRC-PTS for estimating the PAPR of candidate OFDM signals is less than even that of the RC-PTS. Therefore, the IRC-PTS reduces the computational complexity compared to the conventional PTS scheme, previous PTS scheme, and the RC-PTS. Block diagrams of the RC-PTS and the IRC-PTS scheme are shown in Figures 2.13 and 2.14, respectively.

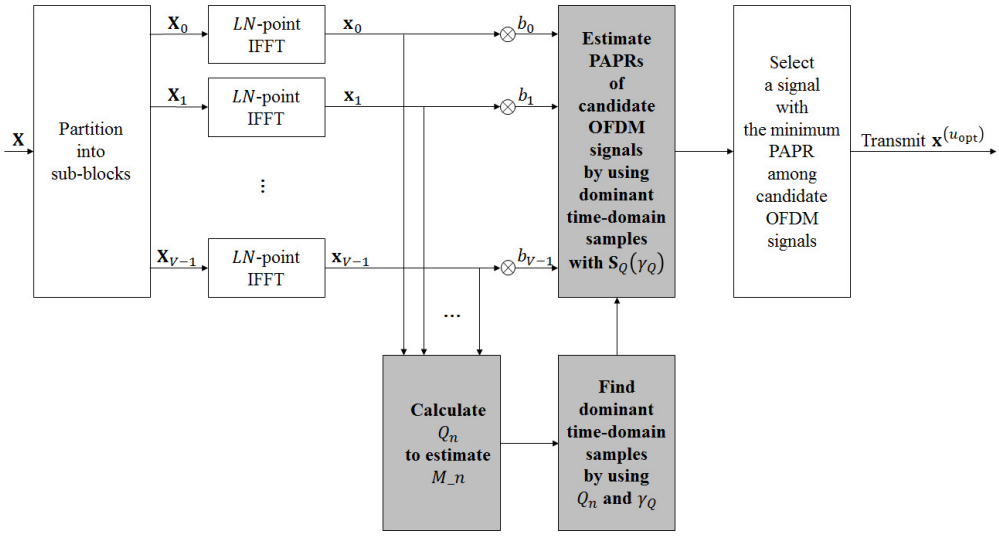

Figure 2.13: A block diagram of RC-PTS.

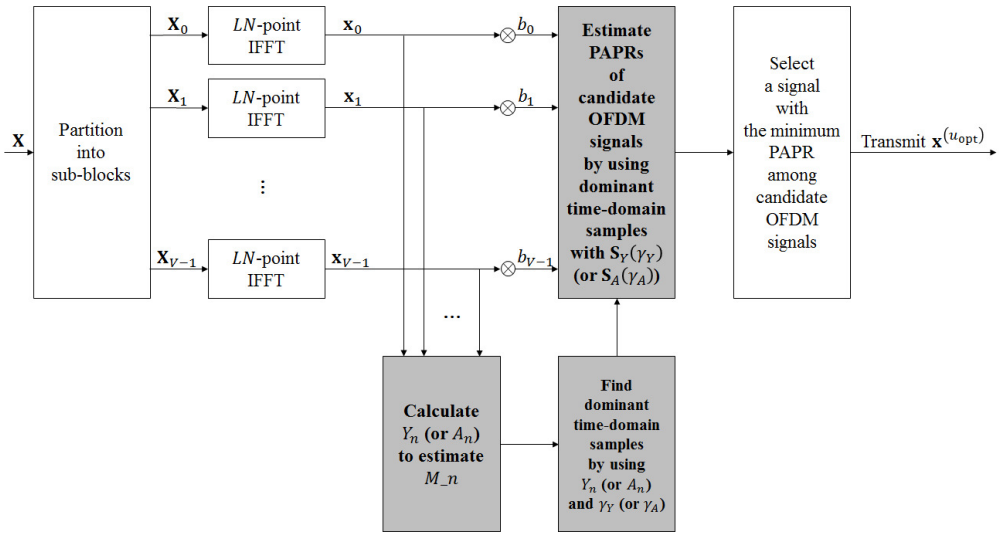

Figure 2.14: A block diagram of IRC-PTS.

Chapter 3

LOW-COMPLEXITY PTS SCHEMES WITH NEW SELECTION METHODS OF DOMINANT TIME-DOMAIN SAMPLES

In this chapter, new PTS schemes with efficient selection methods for dominant time-domain samples are proposed. At first, some notations are introduced for easy understanding of the PTS schemes proposed in this dissertation. Subsequently, new selection methods of candidate samples are proposed to determine the dominant time-domain samples efficiently. Finally, new low-complexity PTS schemes are proposed based on the proposed selection methods of candidate samples for dominant time-domain samples.

3.1 Notations

For easy understanding of the proposed PTS schemes in this chapter and the next chapter, notations for several sub-planes of a two-dimensional complex plane are defined. Ten sub-planes $D_i, 0 \leq i \leq 9$ are defined in Figure 3.1. These sub-planes are utilized to select the candidate samples to estimate the maximum power M_n of samples for all candidate OFDM signals for index n. In addition, four unions of two 45° sub-planes

$E_i, 0 \leq i \leq 3$ are defined in Figure 3.2, where we count the number of the sub-samples $x_{v,n}, 0 \leq v \leq V-1$ in each union E_i for the n-th time-domain sample.

If sub-sample $x_{v,n}$ is located on D_i or E_i, it is denoted as $x_{v,n} \in D_i$ or $x_{v,n} \in E_i$, respectively. For an integer $j, 0 \leq j \leq 7$, $D_i^{(j)}$ or $E_i^{(j)}$ denotes the $j\pi/4$ rotated sub-plane of D_i or E_i, respectively. For all sub-samples $x_{v,n}, 1 \leq v \leq V-1$, except for the first sub-sample $x_{0,n}$ at n, and the sub-planes $E_i, 0 \leq v \leq 3$, the index set for which the sub-samples are located on E_i is represented as

$$\mathbf{V}_n(E_i) = \{v \mid x_{v,n} \in E_i, \quad 1 \leq v \leq V-1\}. \tag{3.1}$$

Subsequently, $\mathbf{V}_n(E_i)$ is utilized to count the number of sub-samples in sub-plane E_i.

3.2 Selection Methods of Candidate Samples for Dominant Time-Domain Samples

In the conventional PTS scheme, M_n denotes the maximum power of the samples among all of the candidate OFDM signals for an index n, which is represented as

$$\begin{aligned} M_n &= \max_{u=0}^{U-1} \left| x_n^{(u)} \right|^2 \\ &= \max_{u=0}^{U-1} \left| \sum_{v=0}^{V-1} b_v^{(u)} x_{v,n} \right|^2, \quad n = 0, 1, \cdots, LN-1 \end{aligned} \tag{3.2}$$

and let $\mathbf{M} = [M_0, M_1, \cdots, M_{LN-1}]$. In other words, M_n indicates the maximum value of the powers obtained from the n-th samples of the U candidate OFDM signals. This implies that the greater M_n indicates a higher probability that the peak power of the candidate OFDM signals occurs at the n-th sample. Therefore, M_n is the proper metric to select the dominant time-domain samples, which is used to estimate the PAPRs of the candidate OFDM signals.

For a preset threshold γ_M, the index set of the dominant time-domain samples is obtained as

$$\mathbf{S}_M(\gamma_M) = \{n \mid M_n \geqslant \gamma_M, \quad 0 \leq n \leq LN-1\}. \tag{3.3}$$

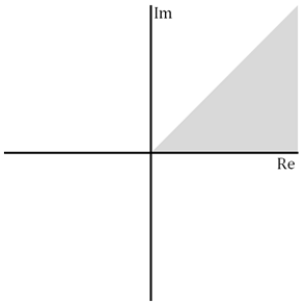

(a) 45° sub-plane D_0

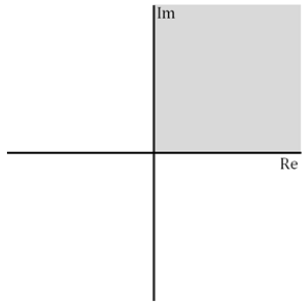

(b) 90° sub-plane D_1

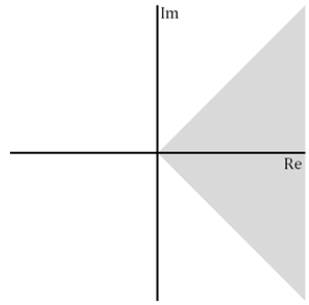

(c) 90° sub-plane D_2

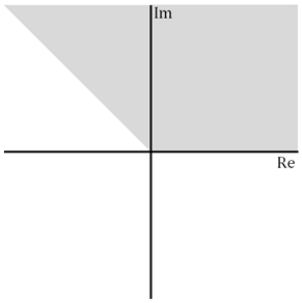

(d) 135° sub-plane D_3

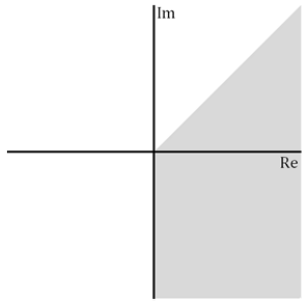

(e) 135° sub-plane D_4

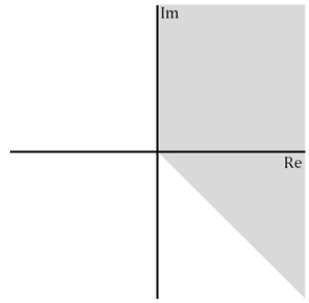

(f) 135° sub-plane D_5

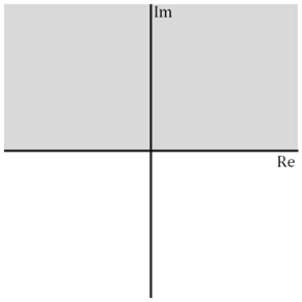

(g) 180° sub-plane D_6

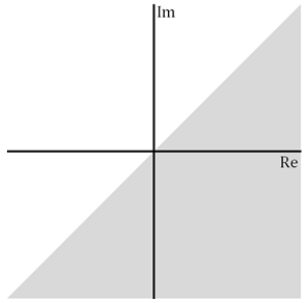

(h) 180° sub-plane D_7

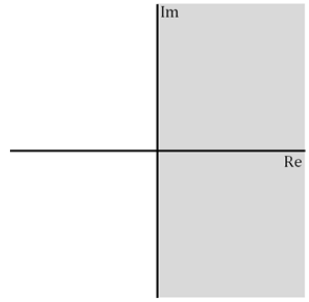

(i) 180° sub-plane D_8

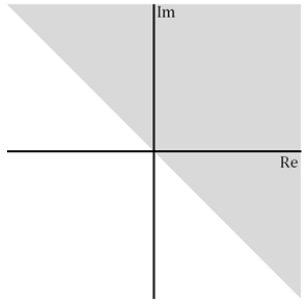

(j) 180° sub-plane D_9

Figure 3.1: Sub-planes of complex plane.

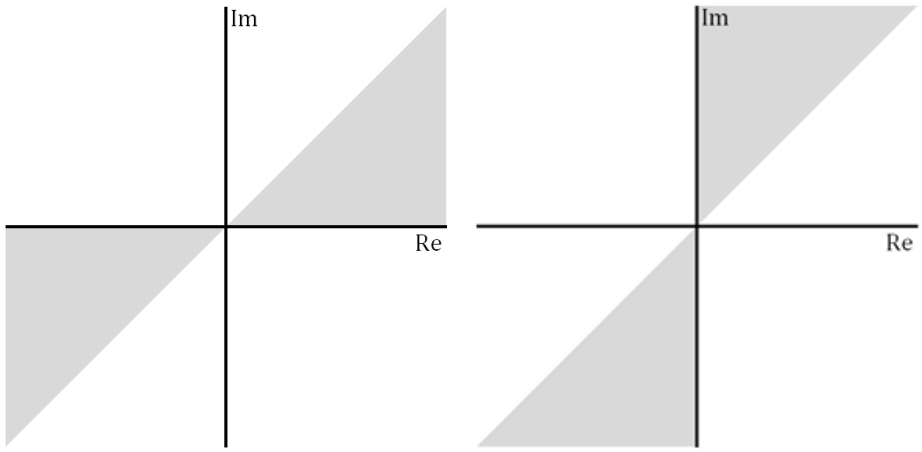

(a) E_0

(b) E_1

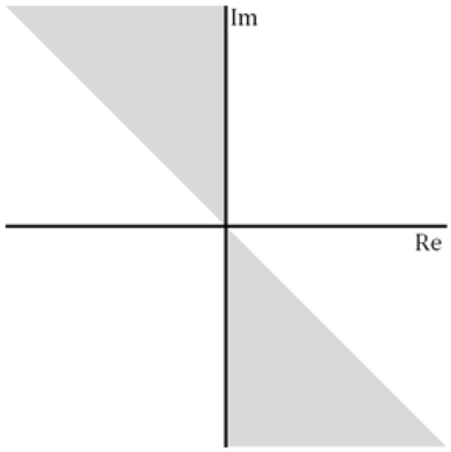

(c) E_2

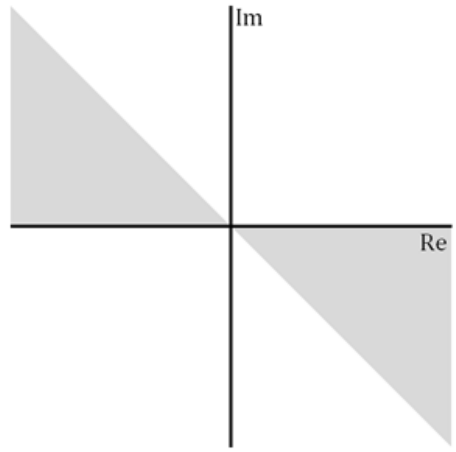

(d) E_3

Figure 3.2: Unions of two 45° sub-planes of complex plane.

Instead of using all time-domain samples, by only using the dominant time-domain samples with indices in $\mathbf{S}_M(\gamma_M)$, the PAPRs of all candidate OFDM signal vectors can be estimated. However, full search over all candidate samples must be performed to find M_n, which requires $U = W^{V-1}$ searches. Note that if $\gamma_M = 0$, $\mathbf{S}_M(\gamma_M)$ is identical to the index set of all time-domain samples, which is used to calculate the PAPR of each candidate OFDM signal in the conventional PTS scheme.

Thus, in this section, we propose new methods to estimate M_n with significantly less computational complexity, where M_n is estimated based on only a few candidate samples multiplied by properly selected phase rotating vectors instead of samples of all candidate signals for index n. In order to select the candidate samples, all of the sub-samples except for the first sub-sample $x_{0,n}$ of the n-th time-domain sample, $x_{v,n}, 1 \leq v \leq V-1$ are rotated to a finite number of the selected sub-planes in which $x_{0,n}$'s are located. These methods will be more clearly explained by using examples as follows.

As the first example, suppose that the first sub-sample $x_{0,n}$ at n is located on the 45° sub-plane D_0 and the other sub-samples $x_{v,n}, 1 \leq v \leq V-1$ are located as shown in Figure 3.3(a). In addition, suppose that $V = 4$ and $W = 2$ are set to generate candidate OFDM signals. In the proposed method, four searches are required to select the candidate samples to estimate M_n, as shown in Figures 3.3(b)–(e), which correspond to $D_i, 6 \leq i \leq 9$, respectively based on the suppositions set above.

In the case of $V = 4$ and $W = 2$, 8 ($= W^{V-1}$) searches are required to estimate the real maximum power M_n of the n-th time-domain sample. However, it is verified through simulation that only four searches such as Figure 3.3(b)–(e) are good enough to find M_n with high probability. Therefore, by using the proposed method to select candidate samples for dominant time-domain samples, the computational complexity to search for a proper signal for transmitting among all candidate OFDM signals is remarkably reduced while keeping almost the same search performance as that of the conventional PTS scheme. Through extensive simulation which counts how many

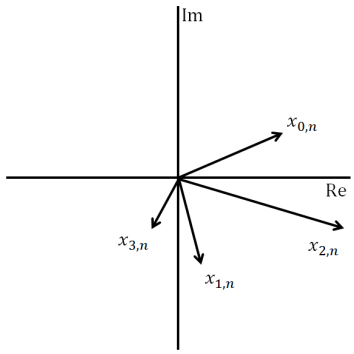

(a) Four sub-samples of the n-th time-domain sample x_n

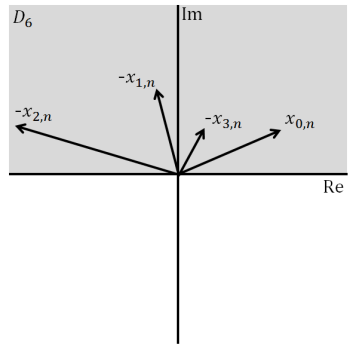

(b) The first search to estimate M_n in the proposed method

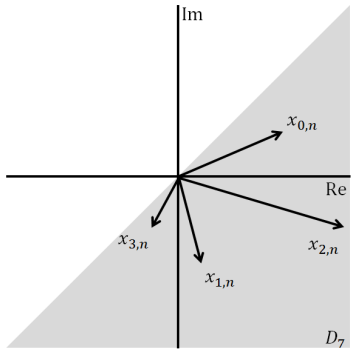

(c) The second search to estimate M_n in the proposed method

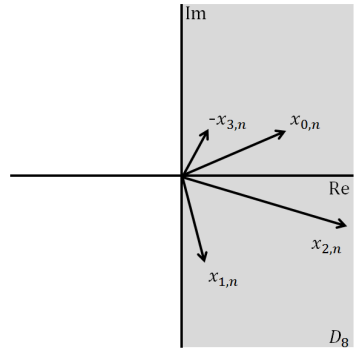

(d) The third search to estimate M_n in the proposed method

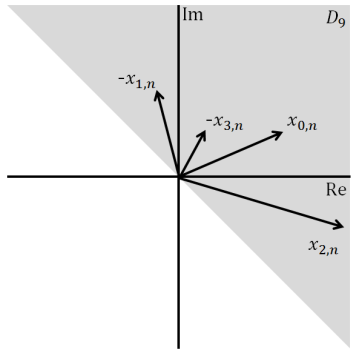

(e) The fourth search to estimate M_n in the proposed method

Figure 3.3: The first example of n-th time-domain sample x_n for $V = 4$ and $W = 2$ in the proposed method to select candidate samples for dominant time-domain samples.

results are matched with M_n by performing searches as in Figure 3.3(b)–(e), the result is that they are matched with the probability 0.997. Note that any number of searches between 1 and 8 by choosing the same number of 180° sub-planes are performed and there is a trade-off between the search performance and the computational complexity.

As the second example, suppose that the first sub-sample $x_{0,n}$ at n is located on the 45° sub-plane D_0 and the other sub-samples $x_{v,n}, 1 \leq v \leq V-1$ are located as shown in Figure 3.4(a). In addition, suppose that $V = 4$ and $W = 4$ are set to generate candidate OFDM signals. Note that W differs in the first and second examples. In the proposed method, two searches are used to select the candidate samples to estimate M_n, as shown in Figures 3.4(b) and (c), which correspond to D_1 and D_2, respectively based on the above settings.

In the case of $W = 4$ such as the condition in Figure 3.4(a), only two searches are performed among $U = W^{V-1} = 64$ searches to estimate M_n of the n-th time-domain sample. It means that in case of $W = 4$, even more computational complexity reduction is achieved than in that of $W = 4$ by using the proposed selection method. Numerical analysis shows that M_n is obtained with the probability 0.903 by two searches in the proposed method with $W = 4$. Note that for the case of $W = 4$ using quaternary phase rotation factors $1, j, -1, -j$, each sub-plane covers 90° sub-planes and the number of searches can be determined by considering the trade-off between the search performance and the computational complexity.

From Figures 3.3 and 3.4, the proposed method to select candidate samples for time-domain samples is explained for the cases of $W = 2$ and $W = 4$. Note that the number of searches is determined by considering W, V, and the trade-off between the search performance and the computational complexity. In detail, among total $U = W^{V-1}$ searches, a proper number of $360^\circ/W$ sub-planes containing $x_{0,n}$ in the complex plane are selected for determining candidate samples to estimate M_n of the n-th time-domain sample.

An index set of U candidate signals is denoted as $\mathbf{Z}_U = \{0, 1, \cdots, U-1\}$. By

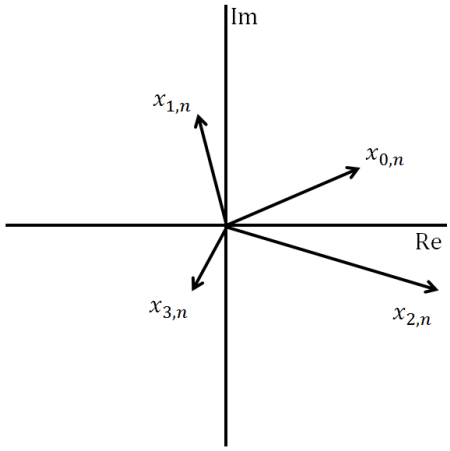

(a) Four sub-samples of the n-th time-domain sample x_n

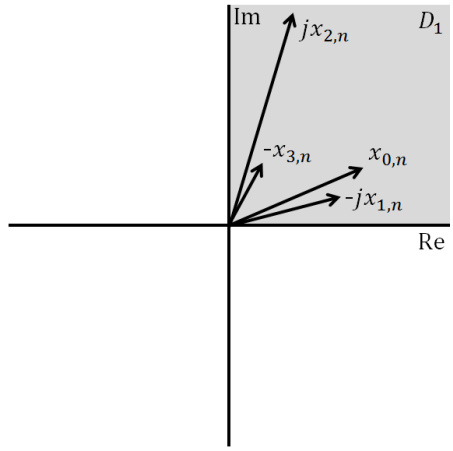

(b) The first search to estimate M_n in the proposed method

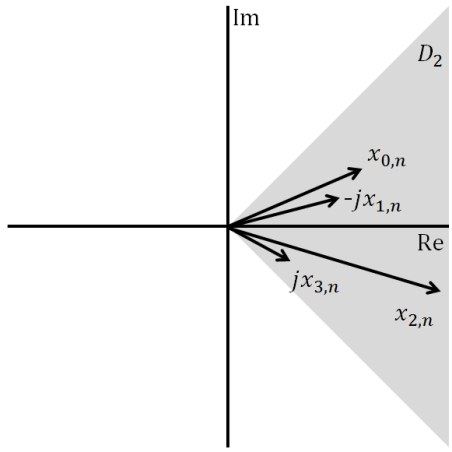

(c) The second search to estimate M_n in the proposed method

Figure 3.4: The second example of n-th time-domain sample x_n for $V = 4$ and $W = 4$ in the proposed method to select candidate samples for dominant time-domain samples.

using the selection method such as Figures 3.3 and 3.4, the powers of C ($= 4$ or 2) candidate samples at n is calculated for estimation of M_n after determining the candidate samples, which are denoted as $x_n^{(K_n(0))}, x_n^{(K_n(1))}, \cdots, x_n^{(K_n(C-1))}$, where $K_n(i) \in \mathbf{Z}_U$ is the index of the candidate samples with the rotated sub-samples located on the sub-plane of $x_{0,n}$. Therefore, a new metric P_n to estimate M_n is proposed as

$$P_n = \max_{c=0}^{C-1} \left| x_n^{(K_n(c))} \right|^2. \tag{3.4}$$

Let $\mathbf{S}_P(\gamma_p)$ be the index set of dominant time-domain samples obtained by using P_n such as

$$\mathbf{S}_P(\gamma_p) = \{n \mid P_n \geqslant \gamma_p, \quad 0 \leq n \leq LN-1\} \tag{3.5}$$

where γ_P is a preset threshold. Then, only the samples with the indices in $\mathbf{S}_P(\gamma_P)$ are used to estimate the PAPR of each candidate OFDM signal. Given that P_n is a good approximation of M_n and a proper metric to select the dominant time-domain samples, a substantial reduction of computational complexity can be achieved with excellent estimation performance.

Now, we evaluate the estimation error of M_n by using P_n through the normalized mean square error (NMSE) defined by

$$NMSE(P_n) = \frac{1}{LN} \sum_{n=0}^{LN-1} \frac{(P_n - M_n)^2}{E[P_n]E[M_n]}. \tag{3.6}$$

Table 3.2 compares the NMSE for the cases of using P_n or Q_n when $C = 4$ (for $W = 2$) or 2 (for $W = 4$), $L = 4$, and $N = 1024$ for various number of sub-blocks V. The NMSE for P_n case is much lower than that for Q_n case regardless of V, which means that P_n approximates M_n more closely compared to Q_n.

The generalized procedures of the proposed methods to select candidate samples for dominant time-domain samples for arbitrary V and W are summarized as follows:

U0) Candidate sub-planes corresponding to candidate samples used to estimate M_n and then select dominant time-dominant samples can be all the $360^\circ/W$ sub-planes containing $x_{0,n}$ in the complex plane for $0 \leq n \leq LN-1$.

Table 3.1: NMSE for estimating M_n by using P_n or Q_n when $N = 1024$ and $L = 4$

Number of sub-blocks (V)	$W = 2$ and $C = 4$		$W = 4$ and $C = 2$	
	P_n	Q_n	P_n	Q_n
4	1.4×10^{-5}	5.4×10^{-3}	1.0×10^{-4}	6.7×10^{-3}
6	4.0×10^{-5}	6.9×10^{-3}	1.4×10^{-4}	8.2×10^{-3}
8	6.6×10^{-5}	7.8×10^{-3}	1.6×10^{-4}	9.1×10^{-3}

U1) Among the candidate sub-planes, select C sub-planes for the proposed selection method such that the boundaries of them are located as far as possible in terms of relative angle at each n.

U2) By using the selected C sub-planes, find the set $\{K_n(0), K_n(1), \cdots, K_n(C-1)\}$ and calculate P_n by using (3.4) at each n.

U3) Construct $\mathbf{S}_P(\gamma_p)$ by using (3.5).

Note that the number of sub-blocks V clearly affects the number of sub-planes C used for the proposed selection method. As V increases, C also increases to keep the search performance. C should be determined by considering the trade-off between the estimation performance and the computational complexity mostly through simulation.

Through exhaust search of simulation, it is concluded that selection methods of candidate samples with $C = 4$ and $C = 2$ have the lowest complexity while achieving the optimal estimation performance for M_n in case of $W = 2$ and $W = 4$ with $V = 4, 6, 8$, respectively. Note that the selection method is different for different value of W. Table **??** represents the summarized the selection methods to select candidate samples to calculate P_n as an estimation of M_n for dominant time-domain samples with the lowest computational complexity and the optimal estimation performance. Note that $C = 2$ and $C = 4$ searches is used to select sub-planes and the corresponding

candidate samples.

Table 3.2: Low-complexity selection methods of candidate samples for dominant time-domain samples

W	Number of selected sub-planes (C)	Selected sub-planes
2	4	$D_6^{(j)}$, $D_7^{(j)}$, $D_8^{(j)}$, and $D_9^{(j)}$
4	2	$D_1^{(j)}$ and $D_2^{(j)}$

3.3 Proposed Low-Complexity PTS Schemes

In this section, new low-complexity PTS schemes with the proposed selection methods for dominant time-domain samples in the previous section are proposed. The proposed PTS scheme, called LC-PTS uses dominant time-domain samples to estimate the PAPR of each candidate OFDM signal.

In LC-PTS, the OFDM signal $\mathbf{x}^{(u_{\text{opt}})}$ selected for transmission is the candidate OFDM signal with index u_{opt} given by

$$u_{\text{opt}} = \arg \min_{u=0}^{U-1} \max_{n \in \mathbf{S}_A(\gamma_A)} \left| \sum_{v=0}^{V-1} b_v^{(u)} x_{v,n} \right|^2 . \tag{3.7}$$

LC-PTS can be summarized with the following steps:

1) Generate candidate OFDM signals $\mathbf{x}^{(u)}, u = 0, 1, \cdots, U-1$.

2) Decide $K_n(c)$'s and then calculate the corresponding P_n's for all $n = 0, 1, \cdots, LN-1$.

3) Based on γ_P and P_n, obtain $\mathbf{S}_P(\gamma_P)$.

4) Among all of the time-domain samples, only the DTDSs with indices in $\mathbf{S}_P(\gamma_P)$ are used to estimate the PAPR of each candidate OFDM signal.

5) Among the candidate OFDM signals, one with the minimum estimated PAPR indexed by u_{opt} is selected and then transmitted as the OFDM signal $\mathbf{x}^{(u_{\text{opt}})}$.

LC-PTS reduces computational complexity considerably while achieving the optimal PAPR reduction performance. A block diagram of the proposed PTS scheme is shown in Figure 3.5.

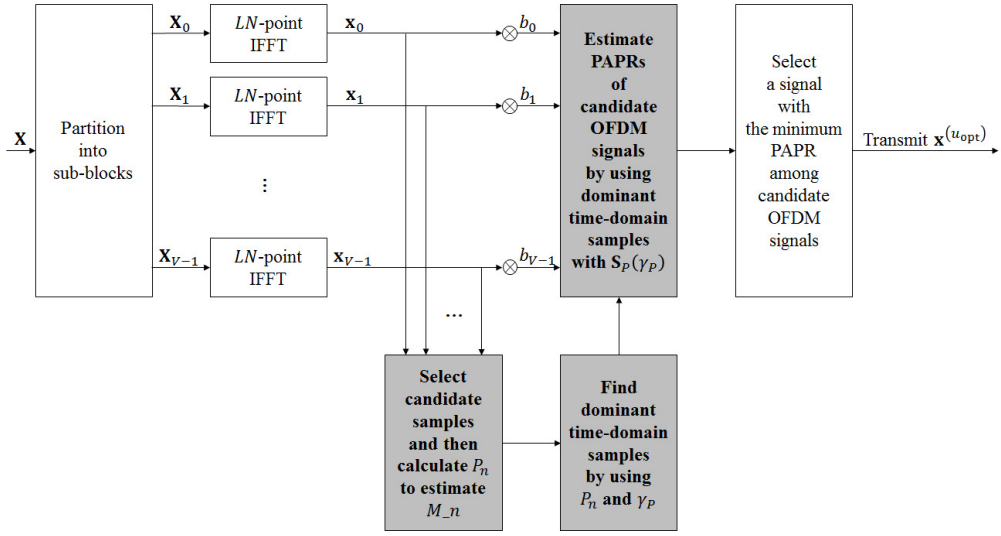

Figure 3.5: A block diagram of LC-PTS.

Chapter 4

IMPROVED PTS SCHEMES WITH ADAPTIVE SELECTION METHODS OF DOMINANT TIME-DOMAIN SAMPLES

In this chpater, three efficient PTS schemes with adaptive selection methods for dominant time-domain samples are proposed. First, the adaptive selection methods of candidate samples are proposed to estimate the dominant time-domain samples efficiently. In addition, a multi-stage selection method for dominant time-domain samples is proposed to reduce the computational complexity further. Finally, the new PTS schemes are proposed based on the proposed selection methods of the dominant time-domain samples.

4.1 Adaptive Selection Methods of Candidate Samples for Dominant Time-Domain Samples

In this section, two adaptive selection methods of candidate samples for dominant time-domain samples are proposed, referred to here as A1-SM and A2-SM. The detailed procedures of A1-SM and A2-SM are described as follows. First, we assume that the first sub-sample $x_{0,n}$ at n is located on $D_0^{(j)}$. Note that the number of searches for

candidate samples at each n in A1-SM and A2-SM can differ, whereas this value is fixed in the LC-PTS proposed in Chapter 3

4.1.1 A1-SM with $W = 2$

A1-SM can be described with the following three steps:

i) For each n, compute the cardinalities of the index sets, $\left|\mathbf{V}_n(E_i^{(j)})\right|, 1 \leq i \leq 3$ in which sub-samples are located on $E_i^{(j)}, 1 \leq i \leq 3$.

ii) Based on $\left|\mathbf{V}_n(E_i^{(j)})\right|$, we adaptively select the sub-planes, where all of the sub-samples can be located on one sub-plane by 180° phase rotation of some of sub-samples among the eight cases presented as below. Note that we disregard the existence of the sub-samples in $E_0^{(j)}$ and the corresponding $\left|\mathbf{V}_n(E_0^{(j)})\right|$ because the first sub-sample $x_{0,n}$ is located on $D_0^{(j)}$, which is already included in $E_0^{(j)}$.

iii) Select each candidate sample obtained by all rotated sub-samples in each selected sub-plane among U candidate samples for each n.

There are eight cases for selection of candidate samples by sub-planes $D_i^{(j)}$ according to $\left|\mathbf{V}_n(E_i^{(j)})\right|$ as follows.

C1-1) $\left|\mathbf{V}_n(E_1^{(j)})\right| = 0$, $\left|\mathbf{V}_n(E_2^{(j)})\right| = 0$, and $\left|\mathbf{V}_n(E_3^{(j)})\right| = 0$;

One candidate sample is selected, where all of the rotated sub-samples are located on the 45° sub-plane $D_0^{(j)}$.

C1-2) $\left|\mathbf{V}_n(E_1^{(j)})\right| = 0$, $\left|\mathbf{V}_n(E_2^{(j)})\right| = 0$, and $\left|\mathbf{V}_n(E_3^{(j)})\right| \geq 1$;

One candidate sample is selected, where all of the rotated sub-samples are located on the 90° sub-plane $D_2^{(j)}$.

C1-3) $\left|\mathbf{V}_n(E_1^{(j)})\right| \geq 1$, $\left|\mathbf{V}_n(E_2^{(j)})\right| = 0$, and $\left|\mathbf{V}_n(E_3^{(j)})\right| = 0$;

One candidate sample is selected, where all of the rotated sub-samples are located on the 90° sub-plane $D_1^{(j)}$.

C1-4) $\left|\mathbf{V}_n(E_1^{(j)})\right| \geq 1$, $\left|\mathbf{V}_n(E_2^{(j)})\right| = 0$, and $\left|\mathbf{V}_n(E_3^{(j)})\right| \geq 1$;

One candidate sample is selected, where all of the rotated sub-samples are located on the 135° sub-plane $D_5^{(j)}$.

C1-5) $\left|\mathbf{V}_n(E_1^{(j)})\right| = 0$, $\left|\mathbf{V}_n(E_2^{(j)})\right| \geq 1$, and $\left|\mathbf{V}_n(E_3^{(j)})\right| = 0$;

Two candidate samples are selected, where all of the rotated sub-samples are located on the 135° sub-planes $D_3^{(j)}$ and $D_4^{(j)}$, respectively.

C1-6) $\left|\mathbf{V}_n(E_1^{(j)})\right| = 0$, $\left|\mathbf{V}_n(E_2^{(j)})\right| \geq 1$, and $\left|\mathbf{V}_n(E_3^{(j)})\right| \geq 1$;

One candidate sample is selected, where all of the rotated sub-samples are located on the 135° sub-plane $D_4^{(j)}$.

C1-7) $\left|\mathbf{V}_n(E_1^{(j)})\right| \geq 1$, $\left|\mathbf{V}_n(E_2^{(j)})\right| \geq 1$, and $\left|\mathbf{V}_n(E_3^{(j)})\right| = 0$;

One candidate sample is selected, where all of the rotated sub-samples are located on the 135° sub-plane $D_3^{(j)}$.

C1-8) $\left|\mathbf{V}_n(E_1^{(j)})\right| \geq 1$, $\left|\mathbf{V}_n(E_2^{(j)})\right| \geq 1$, and $\left|\mathbf{V}_n(E_3^{(j)})\right| \geq 1$;

Four candidate samples are selected, where all of the rotated sub-samples are located on the 180° sub-planes $D_i^{(j)}, 6 \leq i \leq 9$, respectively.

4.1.2 A1-SM with $W = 4$

Similar to the previous case, for each n, compute the sum of the cardinalities of the index sets of which sub-samples are located on $E_1^{(j)}$ and $E_3^{(j)}$, $\left|\mathbf{V}_n(E_1^{(j)})\right| + \left|\mathbf{V}_n(E_3^{(j)})\right|$. Note that we disregard the existence of sub-samples in $E_0^{(j)}$ and $E_2^{(j)}$, as well as the corresponding $\left|\mathbf{V}_n(E_0^{(j)})\right|$ and $\left|\mathbf{V}_n(E_2^{(j)})\right|$ for $W = 4$ because the first sub-sample $x_{0,n}$ is located on $D_0^{(j)}$, which can cover $E_0^{(j)}$ and $E_2^{(j)}$ by itself and its phase rotation in multiples of $\pi/2$. Next, based on $\left|\mathbf{V}_n(E_1^{(j)})\right| + \left|\mathbf{V}_n(E_3^{(j)})\right|$, we adaptively select one or two sub-planes and the corresponding candidate samples in the following two cases.

C2-1) $\left|\mathbf{V}_n(E_1^{(j)})\right| + \left|\mathbf{V}_n(E_3^{(j)})\right| = 0$;

One candidate sample is selected, where all of the rotated sub-samples are located on the 45° sub-plane $D_0^{(j)}$.

C2-2) $\left|\mathbf{V}_n(E_1^{(j)})\right| + \left|\mathbf{V}_n(E_3^{(j)})\right| \geq 1$;

Two candidate samples are selected, where all of the rotated sub-samples are located on the 90° sub-planes $D_1^{(j)}$ and $D_2^{(j)}$, respectively.

4.1.3 A2-SM with $W = 2$

A2-SM considers the additional sub-planes shown in Figure 3.1, possibly including all of the rotated sub-samples compared to A1-SM. For each n, compute the cardinalities of the index sets, $\left|\mathbf{V}_n(E_i^{(j)})\right|, 1 \leq i \leq 3$ for which sub-samples are located on $E_i^{(j)}, 1 \leq i \leq 3$. Next, based on $\left|\mathbf{V}_n(E_i^{(j)})\right|, 1 \leq i \leq 3$, we adaptively select the sub-planes and the corresponding candidate samples in the following eight cases.

C3-1) $\left|\mathbf{V}_n(E_1^{(j)})\right| = 0$, $\left|\mathbf{V}_n(E_2^{(j)})\right| = 0$, and $\left|\mathbf{V}_n(E_3^{(j)})\right| = 0$;

One candidate sample is selected, where all of the rotated sub-samples are located on the 45° sub-plane $D_0^{(j)}$.

C3-2) $\left|\mathbf{V}_n(E_1^{(j)})\right| = 0$, $\left|\mathbf{V}_n(E_2^{(j)})\right| = 0$, and $\left|\mathbf{V}_n(E_3^{(j)})\right| \geq 1$;

One candidate sample is selected, where all of the rotated sub-samples are located on the 90° sub-plane $D_2^{(j)}$.

C3-3) $\left|\mathbf{V}_n(E_1^{(j)})\right| \geq 1$, $\left|\mathbf{V}_n(E_2^{(j)})\right| = 0$, and $\left|\mathbf{V}_n(E_3^{(j)})\right| = 0$;

One candidate sample is selected, where all of the rotated sub-samples are located on the 90° sub-plane $D_1^{(j)}$.

C3-4) $\left|\mathbf{V}_n(E_1^{(j)})\right| \geq 1$, $\left|\mathbf{V}_n(E_2^{(j)})\right| = 0$, and $\left|\mathbf{V}_n(E_3^{(j)})\right| \geq 1$;

Three candidate samples are selected, where all of the rotated sub-samples are located on the sub-planes $D_5^{(j)}$, $D_6^{(j)}$, and $D_7^{(j)}$, respectively.

C3-5) $\left|\mathbf{V}_n(E_1^{(j)})\right| = 0$, $\left|\mathbf{V}_n(E_2^{(j)})\right| \geq 1$, and $\left|\mathbf{V}_n(E_3^{(j)})\right| = 0$;

Two candidate samples are selected, where all of the rotated sub-samples are located on the 135° sub-planes $D_3^{(j)}$ and $D_4^{(j)}$, respectively.

C3-6) $\left|\mathbf{V}_n(E_1^{(j)})\right| = 0$, $\left|\mathbf{V}_n(E_2^{(j)})\right| \geq 1$, and $\left|\mathbf{V}_n(E_3^{(j)})\right| \geq 1$;

Three candidate samples are selected, where all of the rotated sub-samples are located on the sub-planes $D_4^{(j)}$, $D_6^{(j)}$, and $D_9^{(j)}$, respectively.

C3-7) $\left|\mathbf{V}_n(E_1^{(j)})\right| \geq 1$, $\left|\mathbf{V}_n(E_2^{(j)})\right| \geq 1$, and $\left|\mathbf{V}_n(E_3^{(j)})\right| = 0$;

Three candidate samples are selected, where all of the rotated sub-samples are located on the sub-planes $D_3^{(j)}$, $D_7^{(j)}$, and $D_8^{(j)}$, respectively.

C3-8) $\left|\mathbf{V}_n(E_1^{(j)})\right| \geq 1$, $\left|\mathbf{V}_n(E_2^{(j)})\right| \geq 1$, and $\left|\mathbf{V}_n(E_3^{(j)})\right| \geq 1$;

Four candidate samples are selected, where all of the rotated sub-samples are located on the 180° sub-planes $D_i^{(j)}, 6 \leq i \leq 9$, respectively.

It is easy to check that A2-SM selects the candidate samples as the dominant time-domain samples more than that by A1-SM, but it is still less compared to that by LC-PTS. The results of numerical analysis show that A2-SM selects dominant time-domain samples more precisely than A1-SM, but it is nearly identical to that by LC-PTS. Moreover, it is important to note that A2-SM can be used only for the case of $W = 2$. For $W = 4$, it is impossible to select the candidate samples as dominant time-domain samples more than that by A1-SM and less than that by LC-PTS by using an adaptive selection method, that is, A2-SM. For $W = 4$, if we selects the candidate samples as dominant time-domain samples more than that by A1-SM but not adaptively, the candidate samples selected by the selection method becomes the same as that by LC-PTS. The reason for the problem is that sub-planes on which candidate samples is selected by A1-SM is very narrow while that by LC-PTS is wider than A1-SM but still narrow. It means that for $W = 4$, there is no sub-planes on which candidate samples is selected by A2-SM. Therefore, it is concluded that for $W = 4$, it is impossible to

select the candidate samples as dominant time-domain samples by the method similar to A2-SM with $W = 2$ and thus A2-SM is available only for the case of $W = 2$.

As an example, suppose that the first sub-sample $x_{0,n}$ at n is located on the 45° sub-plane D_0 and the other sub-samples $x_{v,n}, 1 \leq v \leq V-1$ are located as shown in Figure 4.1(a). Note that $x_{1,n}$ and $x_{2,n}$ are located on E_3 and $x_{3,n}$ is located on E_0. Then it is easy to check that $\mathbf{V}_n(E_1) = \{1, 2\}$, $\mathbf{V}_n(E_2) = \emptyset$, and $\mathbf{V}_n(E_3) = \emptyset$. In the LC-PTS, four searches are required to select the candidate samples to estimate M_n, as shown in Figures 4.1(b)–(e), which correspond to $D_i, 6 \leq i \leq 9$, respectively. Note that the estimated value of M_n, P_n is used to select dominant time-domain samples as in (3.4) and (3.5). However, in A1-SM or A2-SM, the only one search is needed to select one candidate sample to estimate M_n as shown in Figure 4.1(f), which corresponds to D_1. Thus, the proposed selection methods can reduce the search complexity by one quarter when selecting candidate samples to estimate M_n compared to that by the LC-PTS.

As an additional example, suppose that the first sub-sample $x_{0,n}$ at n is located on the 45° sub-plane D_0 and the other sub-samples $x_{v,n}, 1 \leq v \leq V-1$ are located as shown in Figure 4.2(a). Note that $x_{1,n}$ and $x_{2,n}$ are located on E_2 and $x_{3,n}$ is located on E_0. Then it is easy to check that $\mathbf{V}_n(E_1) = \emptyset$, $\mathbf{V}_n(E_2) = \{1, 2\}$, and $\mathbf{V}_n(E_3) = \emptyset$. With LC-PTS, four searches are required to select candidate samples to estimate M_n, as shown in Figures 4.2(b)–(e), which correspond to $D_i, 6 \leq i \leq 9$, respectively. On the other hand, in A1-SM or A2-SM, two searches are needed to select candidate samples to estimate M_n, as shown in Figures 4.2(f) and (g), which correspond to D_3 and D_4, respectively. Thus, the proposed selection methods can reduce the search complexity by half when selecting candidate samples to estimate M_n, compared to that by LC-PTS.

One additional example is considered in Figure 4.3 to explain a different selection case of the proposed selection methods for candidate samples. Suppose that the first sub-sample $x_{0,n}$ at n is located on the 45° sub-plane D_0 and the other sub-samples $x_{v,n}, 1 \leq v \leq V-1$ are located as shown in Figure 4.3(a). Note that $x_{1,n}$ is located on

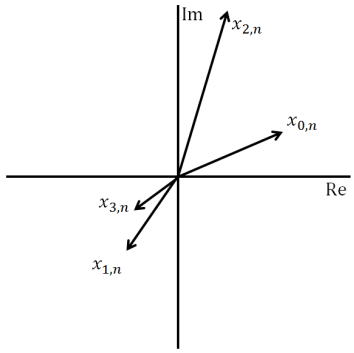

(a) Four sub-samples of the n-th time-domain sample x_n

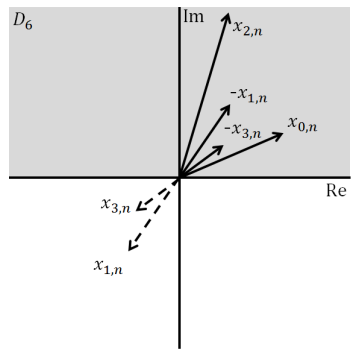

(b) The first search to estimate M_n in the LC-PTS

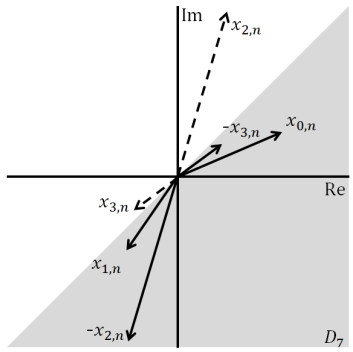

(c) The second search to estimate M_n in the LC-PTS

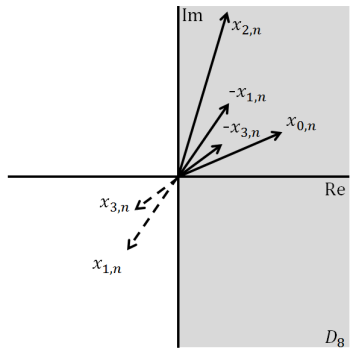

(d) The third search to estimate M_n in the LC-PTS

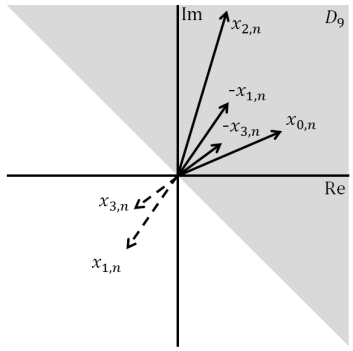

(e) The fourth search to estimate M_n in the LC-PTS

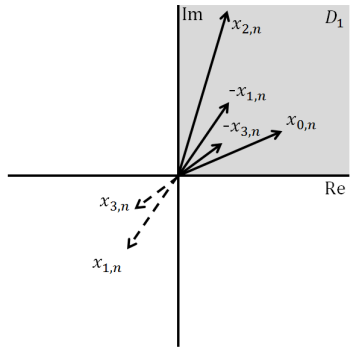

(f) One search of A1-SM or A2-SM to estimate M_n

Figure 4.1: The first example of n-th time-domain sample x_n for $V = 4$ and $W = 2$.

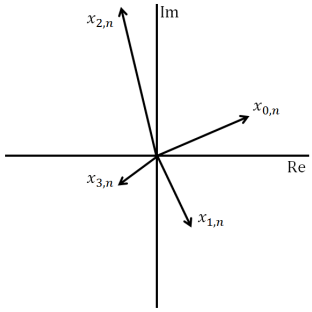

(a) Four sub-samples of the n-th time-domain sample x_n

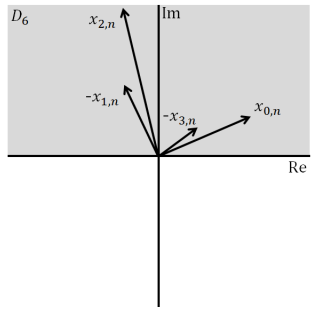

(b) The first search to estimate M_n in the LC-PTS

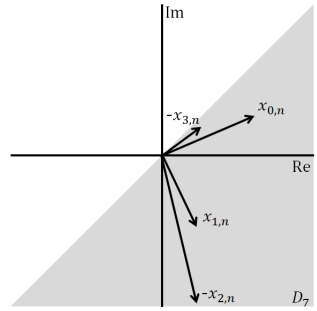

(c) The second search to estimate M_n in the LC-PTS

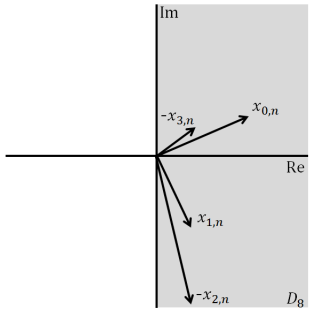

(d) The third search to estimate M_n in the LC-PTS

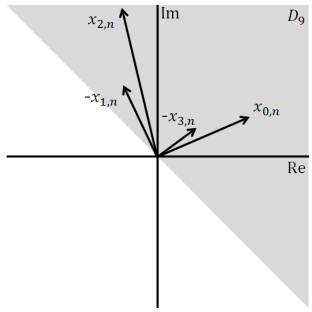

(e) The fourth search to estimate M_n in the LC-PTS

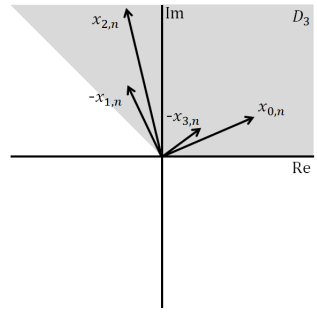

(f) The first search of A1-SM or A2-SM to estimate M_n

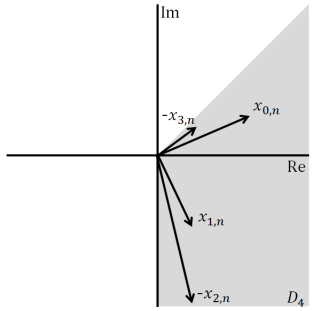

(g) The second search of A1-SM or A2-SM to estimate M_n

Figure 4.2: The second example of n-th time-domain sample x_n for $V = 4$ and $W = 2$.

E_1 and $x_{2,n}$ and $x_{3,n}$ are located on E_3. Then, it is easy to check that $\mathbf{V}_n(E_1) = \{1\}$, $\mathbf{V}_n(E_2) = \emptyset$, and $\mathbf{V}_n(E_3) = \{2, 3\}$. In LC-PTS, four searches are required to select candidate samples to estimate M_n, as shown in Figures 4.3(b)–(e), corresponding to $D_i, 6 \leq i \leq 9$, respectively. However, in A1-SM, only one search is needed to select one candidate sample to estimate M_n, as shown in Figure 4.3(f), corresponding to D_5. In A2-SM, three searches are needed to select candidate samples to estimate M_n, as shown in Figures 4.3(g)–(i), corresponding to $D_i, 5 \leq i \leq 7$, respectively. Note that the candidate rotation set of A2-SM includes that of A1-SM in this example. Thus, A1-SM and A2-SM can reduce the search complexity by one quarter and three quarters, respectively, when selecting candidate samples to estimate M_n, as compared to that by LC-PTS.

The three examples described above imply that A1-SM and A2-SM reduce the number of searches required for selection of the candidate samples compared to that by LC-PTS. Let C_n be the number of searches for the candidate samples at n. In order to show how effectively A1-SM and A2-SM reduce the number of searches for the candidate samples, Table 4.1 shows a probability distribution for cases in which A1-SM and A2-SM use C_n searches to select the candidate samples at n. Without a loss of generality, we assume that the first sub-sample $x_{0,n}$ at n is located on $D_0^{(j)}$. Also, it is assumed that the length of the oversampled input symbol vector and the corresponding OFDM signal vector LN is large enough such that law of large numbers can be applied. The results in Table 4.1 are obtained by both computing the mathematical representations in Table 4.1(a) and conducting numerical analysis in Table 4.1(b) and we can verify that these two results are identical. It is straightforward to check that the probability of C_n is dependent only on the number of sub-blocks, V. Note that C_n takes value 1, 2, or 4 in A1-SM with $W = 2$ and value 1, 2, 3, or 4 in A2-SM with $W = 2$, respectively. On the other hand, in A1-SM with $W = 4$, C_n takes value 1 or 2. The next section shows how the mathematical representations of the probability distribution of C_n for n are formulated in detail.

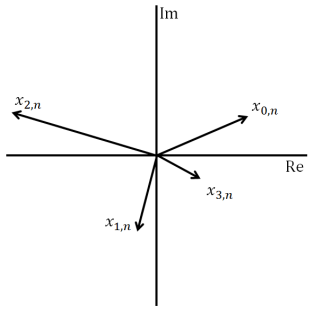

(a) Four sub-samples of the n-th time-domain sample x_n

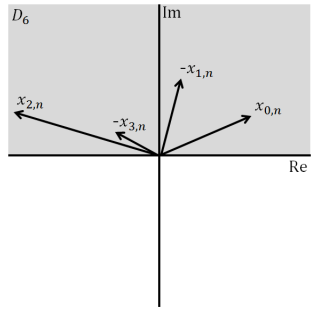

(b) The first search to estimate M_n in the LC-PTS

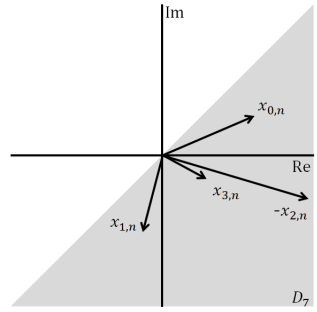

(c) The second search to estimate M_n in the LC-PTS

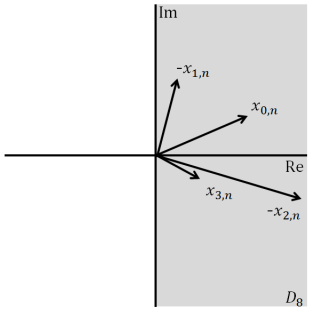

(d) The third search to estimate M_n in the LC-PTS

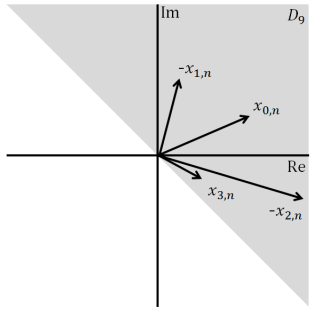

(e) The fourth search to estimate M_n in the LC-PTS

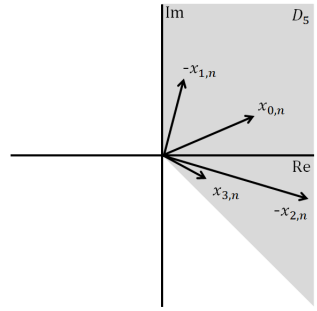

(f) One search of A1-SM to estimate M_n

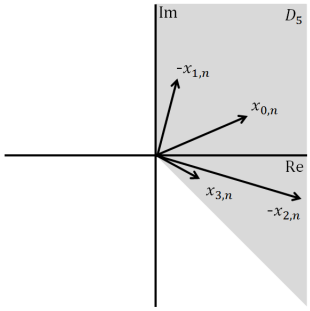

(g) The first search of A2-SM to estimate M_n

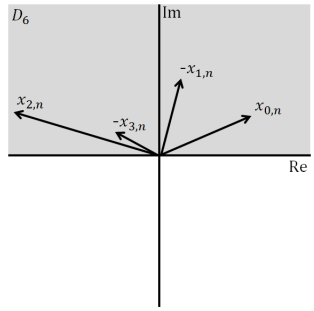

(h) The second search of A2-SM to estimate M_n

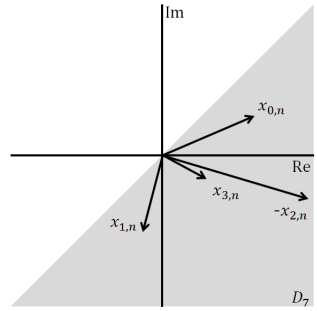

(i) The third search of A2-SM to estimate M_n

Figure 4.3: The third example of n-th time-domain sample x_n for $V = 4$ and $W = 2$.

Table 4.1: Probability distribution of C_n

(a) Mathematical representations

C_n	Probability of C_n		
	A1-SM with $W = 2$	A1-SM with $W = 2$	A1-SM with $W = 2$
1	$3\left(\frac{3}{4}\right)^{V-1} - 4\left(\frac{1}{2}\right)^{V-3} + 2\left(\frac{1}{4}\right)^{V-1}$	$\left(\frac{1}{2}\right)^{V-2} - \left(\frac{1}{4}\right)^{V-1}$	$\left(\frac{1}{2}\right)^{V-1}$
2	$\left(\frac{1}{2}\right)^{V-1} - \left(\frac{1}{4}\right)^{V-1}$	$\left(\frac{1}{2}\right)^{V-1} - \left(\frac{1}{4}\right)^{V-1}$	$1 - \left(\frac{1}{2}\right)^{V-1}$
3	0	$3\left(\frac{3}{4}\right)^{V-1} - 3\left(\frac{1}{2}\right)^{V-2} + 3\left(\frac{1}{4}\right)^{V-1}$	0
4	$1 - 3\left(\frac{3}{4}\right)^{V-1} + 3\left(\frac{1}{2}\right)^{V-1} - \left(\frac{1}{4}\right)^{V-1}$	$1 - 3\left(\frac{3}{4}\right)^{V-1} + 3\left(\frac{1}{2}\right)^{V-1} - \left(\frac{1}{4}\right)^{V-1}$	0

(b) Simulation results

V	C_n	Probability of C_n		
		A1-SM with $W = 2$	A1-SM with $W = 2$	A1-SM with $W = 2$
4	1	0.7968	0.2344	0.125
	2	0.1094	0.1094	0.875
	3	0	0.5624	0
	4	0.0938	0.0938	0
8	1	0.3693	0.0156	0.0078
	2	0.0078	0.0078	0.9922
	3	0	0.3537	0
	4	0.6229	0.6229	0

The proposed selection methods A1-SM and A2-SM for candidate samples are summarized in Tables 4.2 and 4.3, respectively. Note that we disregard $\left|\mathbf{V}_n(E_0^{(j)})\right|$ when assessing the conditions for A1-SM and A2-SM and ignore $\left|\mathbf{V}_n(E_1^{(j)})\right|$ when checking the conditions for A1-SM with $W = 4$.

Table 4.2: Selection method of A1-SM

(a) $W = 2$

Cases	Conditions			Selection methods	
	$\left\|\mathbf{V}_n(E_1^{(j)})\right\|$	$\left\|\mathbf{V}_n(E_2^{(j)})\right\|$	$\left\|\mathbf{V}_n(E_3^{(j)})\right\|$	Selected sub-planes	Number of searches
C1-1	0	0	0	$D_0^{(j)}$	1
C1-2	0	0	≥ 1	$D_2^{(j)}$	1
C1-3	≥ 1	0	0	$D_1^{(j)}$	1
C1-4	≥ 1	0	≥ 1	$D_5^{(j)}$	1
C1-5	0	≥ 1	0	$D_3^{(j)}$, $D_4^{(j)}$	2
C1-6	0	≥ 1	≥ 1	$D_4^{(j)}$	1
C1-7	≥ 1	≥ 1	0	$D_3^{(j)}$	1
C1-8	≥ 1	≥ 1	≥ 1	$D_6^{(j)}$, $D_7^{(j)}$, $D_8^{(j)}$, $D_9^{(j)}$	4

(b) $W = 4$

Cases	Conditions	Selection methods	
	$\left\|\mathbf{V}_n(E_1^{(j)})\right\| + \left\|\mathbf{V}_n(E_3^{(j)})\right\|$	Selected sub-planes	Number of searches
C2-1	0	$D_0^{(j)}$	1
C2-2	≥ 1	$D_1^{(j)}$, $D_2^{(j)}$	2

After A1-SM or A2-SM, M_n is estimated to select the dominant time-domain samples. Let S_n be the maximum power of the candidate samples selected by A1-SM

Table 4.3: Selection method of A2-SM with $W = 2$

Cases	Conditions			Selection methods	
	$\left\|\mathbf{V}_n(E_1^{(j)})\right\|$	$\left\|\mathbf{V}_n(E_2^{(j)})\right\|$	$\left\|\mathbf{V}_n(E_3^{(j)})\right\|$	Selected sub-planes	Number of searches
C3-1	0	0	0	$D_0^{(j)}$	1
C3-2	0	0	≥ 1	$D_2^{(j)}$	1
C3-3	≥ 1	0	0	$D_1^{(j)}$	1
C3-4	≥ 1	0	≥ 1	$D_5^{(j)}$, $D_6^{(j)}$, $D_7^{(j)}$	3
C3-5	0	≥ 1	0	$D_3^{(j)}$ and $D_4^{(j)}$	2
C3-6	0	≥ 1	≥ 1	$D_4^{(j)}$, $D_6^{(j)}$, $D_9^{(j)}$	3
C3-7	≥ 1	≥ 1	0	$D_3^{(j)}$, $D_7^{(j)}$, $D_8^{(j)}$	3
C3-8	≥ 1	≥ 1	≥ 1	$D_6^{(j)}$, $D_7^{(j)}$, $D_8^{(j)}$, $D_9^{(j)}$	4

or A2-SM, which is considered to be the estimated value of M_n. Table 4.4 shows how accurately S_n can estimate M_n in LC-PTS, A1-SM, and A2-SM, where OFDM signals with $N = 256, 1024$, 16-QAM, $L = 4$, and $W = 2$ are considered. For the evaluation, the estimation error rate of M_n is defined as the ratio of the number of samples with an estimation error of M_n to the total number of time-domain samples. In Table 4.4, the accuracy of the estimation of M_n by A2-SM is better than that by A1-SM and nearly identical to that by LC-PTS.

Table 4.4: Accuracy performance for estimation of M_n for 16-QAM, $L = 4$, and $W = 2$

(a) $V = 4$

Estimation methods	Estimation error rate of samples	
	$N = 256$	$N = 1024$
P_n (LC-SM)	0.26%	0.26%
S_n (A1-SM)	9.68%	9.68%
S_n (A2-SM)	0.26%	0.26%

(b) $V = 8$

Estimation methods	Estimation error rate of samples	
	$N = 256$	$N = 1024$
P_n (LC-SM)	5.88%	5.89%
S_n (A1-SM)	9.50%	9.50%
S_n (A2-SM)	5.89%	5.89%

After M_n is estimated as S_n for each n, the dominant time-domain samples are selected using S_n as the metric. The index set of the dominant time-domain samples

obtained using S_n is denoted as

$$\mathbf{S}_S(\gamma_S) = \{n \mid S_n \geq \gamma_S, \quad 0 \leq n \leq LN-1\} \tag{4.1}$$

where γ_S is a preset threshold. Then, only the samples with indices in $\mathbf{S}_S(\gamma_S)$ are used to estimate the PAPR of each candidate OFDM signal. Since S_n is an accurate approximation of M_n, the selection method of the time-domain samples can achieve considerable reduction of the computational complexity to determine the PAPR of the candidate OFDM signals.

4.2 Mathematical Representations for Probability Distribution of C_n

Without a loss of generality, we assume that the first sub-sample $x_{0,n}$ at n is located on $D_0^{(j)}$. In addition, we assume that the length of the oversampled input symbol vector and the corresponding OFDM signal vector, LN, is large enough such that the law of large numbers applies. In this case, according to the law of large numbers, all $\Pr(x_{v,n} \in E_i)$' values are approximately equal, that is, $\Pr(x_{v,n} \in E_i) \approx 1/8$ for $0 \leq v \leq V-1$ and $0 \leq n \leq LN-1$. Let x be a random variable of complex values uniformly distributed on a two-dimensional complex plane.

The probabilities of all cases of the proposed selection methods are represented as follows. Note that the probabilities of the cases in A1-SM and A2-SM with $W = 2$ are the same as;

$$\begin{aligned}
\Pr(\text{C1-1}) &= \Pr(\text{C3-1}) \\
&= \sum_{j=0}^{7} \Pr\left(x \in D_0^{(j)}\right) \left[\Pr\left(x \in E_0^{(j)}\right)\right]^{V-1} \\
&= \left(\frac{1}{4}\right)^{V-1}
\end{aligned} \tag{4.2}$$

$$
\begin{aligned}
\Pr\left(\text{C1-2}\right) &= \Pr\left(\text{C3-2}\right) \\
&= \sum_{j=0}^{7} \Pr\left(x \in D_0^{(j)}\right) \left[\left[\Pr\left(x \in E_0^{(j)} \cup E_1^{(j)}\right)\right]^{V-1}\right. \\
&\quad \left. -\left[\Pr\left(x \in E_0^{(j)}\right)\right]^{V-1}\right] \\
&= \left(\frac{1}{2}\right)^{V-1} - \left(\frac{1}{4}\right)^{V-1}
\end{aligned} \tag{4.3}
$$

$$
\begin{aligned}
\Pr\left(\text{C1-3}\right) &= \Pr\left(\text{C3-3}\right) \\
&= \sum_{j=0}^{7} \Pr\left(x \in D_0^{(j)}\right) \left[\left[\Pr\left(x \in E_0^{(j)} \cup E_3^{(j)}\right)\right]^{V-1}\right. \\
&\quad \left. -\left[\Pr\left(x \in E_0^{(j)}\right)\right]^{V-1}\right] \\
&= \left(\frac{1}{2}\right)^{V-1} - \left(\frac{1}{4}\right)^{V-1}
\end{aligned} \tag{4.4}
$$

$$
\begin{aligned}
\Pr\left(\text{C1-4}\right) &= \Pr\left(\text{C3-4}\right) \\
&= \sum_{j=0}^{7} \Pr\left(x \in D_0^{(j)}\right) \left[\sum_{i=2}^{V-1} \left[\Pr\left(x \in \left(E_2^{(j)}\right)^c\right)\right]^{V-i-1}\right. \\
&\quad \left.\left[\sum_{k=1}^{i-1} \binom{i}{k} \left[\Pr\left(x \in E_1^{(j)}\right)\right]^{k-1} \left[\Pr\left(x \in E_3^{(j)}\right)\right]^{i-k+1}\right]\right] \\
&= \left(\frac{3}{4}\right)^{V-1} - 2\left(\frac{1}{2}\right)^{V-3} + \left(\frac{1}{4}\right)^{V-1}
\end{aligned} \tag{4.5}
$$

$$
\begin{aligned}
\Pr\left(\text{C1-5}\right) &= \Pr\left(\text{C3-5}\right) \\
&= \sum_{j=0}^{7} \Pr\left(x \in D_0^{(j)}\right) \left[\sum_{i=1}^{V-1} \binom{V-1}{i} \left[\Pr\left(x \in E_2^{(j)}\right)\right]^{i}\right. \\
&\quad \left.\left[\Pr\left(x \in E_0^{(j)}\right)\right]^{V-i-1}\right] \\
&= \left(\frac{1}{2}\right)^{V-1} + \left(\frac{1}{4}\right)^{V-1}
\end{aligned} \tag{4.6}
$$

$$
\begin{aligned}
\Pr(\text{C1-6}) &= \Pr(\text{C3-6}) \\
&= \sum_{j=0}^{7} \Pr\left(x \in D_0^{(j)}\right) \left[\sum_{i=2}^{V-1} \left[\Pr\left(x \in \left(E_1^{(j)}\right)^c\right)\right]^{V-i-1}\right. \\
&\quad \left.\left[\sum_{k=1}^{i-1} \binom{i}{k} \left[\Pr\left(x \in E_2^{(j)}\right)\right]^{k-1} \left[\Pr\left(x \in E_3^{(j)}\right)\right]^{i-k+1}\right]\right] \qquad (4.7) \\
&= \left(\frac{3}{4}\right)^{V-1} - 2\left(\frac{1}{2}\right)^{V-3} + \left(\frac{1}{4}\right)^{V-1}
\end{aligned}
$$

$$
\begin{aligned}
\Pr(\text{C1-7}) &= \Pr(\text{C3-7}) \\
&= \sum_{j=0}^{7} \Pr\left(x \in D_0^{(j)}\right) \left[\sum_{i=2}^{V-1} \left[\Pr\left(x \in \left(E_3^{(j)}\right)^c\right)\right]^{V-i-1}\right. \\
&\quad \left.\left[\sum_{k=1}^{i-1} \binom{i}{k} \left[\Pr\left(x \in E_1^{(j)}\right)\right]^{k-1} \left[\Pr\left(x \in E_2^{(j)}\right)\right]^{i-k+1}\right]\right] \qquad (4.8) \\
&= \left(\frac{3}{4}\right)^{V-1} - 2\left(\frac{1}{2}\right)^{V-3} + \left(\frac{1}{4}\right)^{V-1}
\end{aligned}
$$

$$
\begin{aligned}
\Pr(\text{C1-8}) &= \Pr(\text{C3-8}) \\
&= 1 - [\Pr(\text{C1-1}) + \Pr(\text{C1-2}) + \Pr(\text{C1-3}) + \Pr(\text{C1-4}) \\
&\quad + \Pr(\text{C1-5}) + \Pr(\text{C1-6}) + \Pr(\text{C1-7})] \qquad (4.9) \\
&= \left(\frac{3}{4}\right)^{V-1} - 2\left(\frac{1}{2}\right)^{V-3} + \left(\frac{1}{4}\right)^{V-1}
\end{aligned}
$$

$$
\begin{aligned}
\Pr(\text{C2-1}) &= \sum_{j=0}^{7} \Pr\left(x \in D_0^{(j)}\right) \left[\Pr\left(x \in E_0^{(j)} \cup E_2^{(j)}\right)\right]^{V-1} \\
&= \left(\frac{1}{2}\right)^{V-1} \qquad (4.10)
\end{aligned}
$$

$$
\begin{aligned}
\Pr(\text{C2-2}) &= 1 - \Pr(\text{C2-1}) \\
&= 1 - \left(\frac{1}{2}\right)^{V-1} \qquad (4.11)
\end{aligned}
$$

Based on the probabilities of all cases of the proposed selection methods of the candidate selection methods, the probabilities of C_n are represented as follows.

4.2.1 A1-SM with $W = 2$

In A1-SM with $W = 2$, the probabilities of C_n are derived as follows:

$$\begin{aligned}\Pr(C_n = 1) &= \Pr(\text{C1-1}) + \Pr(\text{C1-2}) + \Pr(\text{C1-3}) + \Pr(\text{C1-4}) \\ &\quad + \Pr(\text{C1-6}) + \Pr(\text{C1-7}) \\ &= 3\left(\frac{3}{4}\right)^{V-1} - 4\left(\frac{1}{2}\right)^{V-3} + 2\left(\frac{1}{4}\right)^{V-1} + \Pr(\text{C1-4})\end{aligned} \tag{4.12}$$

$$\begin{aligned}\Pr(C_n = 2) &= \Pr(\text{C1-5}) \\ &= \left(\frac{1}{2}\right)^{V-1} - \left(\frac{1}{4}\right)^{V-1}\end{aligned} \tag{4.13}$$

$$\begin{aligned}\Pr(C_n = 4) &= \Pr(\text{C1-8}) \\ &= 1 - 3\left(\frac{3}{4}\right)^{V-1} + 3\left(\frac{1}{2}\right)^{V-1} - \left(\frac{1}{4}\right)^{V-1}\end{aligned} \tag{4.14}$$

4.2.2 A1-SM with $W = 4$

In A1-SM with $W = 4$, the probabilities of C_n are derived as follows:

$$\begin{aligned}\Pr(C_n = 1) &= \Pr(\text{C2-1}) \\ &= \left(\frac{1}{2}\right)^{V-1}\end{aligned} \tag{4.15}$$

$$\begin{aligned}\Pr(C_n = 2) &= \Pr(\text{C2-2}) \\ &= 1 - \left(\frac{1}{2}\right)^{V-1}\end{aligned} \tag{4.16}$$

4.2.3 A2-SM with $W = 2$

In A2-SM with $W = 2$, the probabilities of C_n are derived as follows:

$$\begin{aligned}\Pr(C_n = 1) &= \Pr(\text{C3-1}) + \Pr(\text{C3-2}) + \Pr(\text{C3-3}) \\ &= \left(\frac{1}{2}\right)^{V-2} - \left(\frac{1}{4}\right)^{V-1}\end{aligned} \tag{4.17}$$

$$\begin{aligned}\Pr(C_n = 2) &= \Pr(\text{C3-5}) \\ &= \left(\frac{1}{2}\right)^{V-1} - \left(\frac{1}{4}\right)^{V-1}\end{aligned} \tag{4.18}$$

$$\begin{aligned}\Pr(C_n = 3) &= \Pr(\text{C3-4}) + \Pr(\text{C3-6}) + \Pr(\text{C3-7}) \\ &= 3\left(\frac{3}{4}\right)^{V-1} - 3\left(\frac{1}{2}\right)^{V-2} + 3\left(\frac{1}{4}\right)^{V-1}\end{aligned} \tag{4.19}$$

$$\begin{aligned}\Pr(C_n = 4) &= \Pr(\text{C3-8}) \\ &= 1 - 3\left(\frac{3}{4}\right)^{V-1} + 3\left(\frac{1}{2}\right)^{V-1} - \left(\frac{1}{4}\right)^{V-1}\end{aligned} \tag{4.20}$$

4.3 Multi-Stage Selection Method of Dominant Time-Domain Samples

In this section, a more advanced multi-stage selection method (M-SM) is proposed for the selection of the dominant time-domain samples. M-SM has two stages, with the first stage using the selection method A1-SM or A2-SM for the candidate samples in the previous section and the second stage using the selection method of the candidate samples proposed in the LC-PTS. In the first stage of M-SM, a larger set of dominant time-domain samples is selected among all samples using the selection method A1-SM or A2-SM. Note that the dominant time-domain samples selected in the first stage are only a fraction of all samples but much larger than the number of dominant time-domain samples selected in the second stage. After the first stage, the second set of dominant time-domain samples is selected among the first set of dominant time-domain samples using the selection method of the LC-PTS in the second stage.

In M-SM, the index set of the dominant time-domain samples in the first stage is defined as

$$\mathbf{S}_1(\beta_T) = \{n \mid S_n \geq \beta_T, \quad 0 \leq n \leq LN - 1\} \tag{4.21}$$

where β_T is a preset threshold of the first stage. Note that $\mathbf{S}_1(\beta_T)$ is obtained by using S_n. In addition, the index set of the dominant time-domain samples in the second stage is represented by $\mathbf{S}_T(\gamma_T)$, which is obtained as

$$\mathbf{S}_T(\gamma_T) = \{n \mid P_n \geq \gamma_T, \quad n \in \mathbf{S}_1(\beta_T)\} \tag{4.22}$$

where γ_T is a preset threshold of the second stage. It is easy to verify whether $\mathbf{S}_T(\gamma_T)$ is obtained by using P_n in (3.4) among only the samples whose index set is $\mathbf{S}_1(\beta_T)$.

With M-SM, the second set of dominant time-domain samples required to estimate M_n precisely is reduced further compared to that by A1-SM or A2-SM in the previous section. Therefore, M-SM can lower the computational complexity of PTS schemes further using the dominant time-domain samples while maintaining the optimal PAPR reduction performance.

4.4 Proposed PTS Schemes with Adaptive Selection Methods for Dominant Time-Domain Samples

In this section, two types of PTS schemes with adaptive selection methods for dominant time-domain samples are proposed. The first type of PTS scheme, called A-PTS, are based on the selection methods A1-SM and A2-SM. On the other hand, the other type of PTS scheme, called M-PTS, is based on the selection method M-SM. All of the proposed PTS schemes use dominant time-domain samples to determine the PAPR of each candidate OFDM signal. However, A-PTS uses dominant time-domain samples whose index set is $\mathbf{S}_S(\gamma_S)$ in (4.1), while M-PTS uses the dominant time-domain samples whose index set is $\mathbf{S}_T(\gamma_T)$ in (4.22).

In A-PTS, the OFDM signal $\mathbf{x}^{(u_{\text{opt}})}$ selected for transmission is the candidate OFDM signal with index $u_{\text{opt},A}$ given by

$$u_{\text{opt},S} = \arg \min_{u=0}^{U-1} \max_{n \in \mathbf{S}_S(\gamma_S)} \left| \sum_{v=0}^{V-1} b_v^{(u)} x_{v,n} \right|^2 . \tag{4.23}$$

On the other hand, the OFDM signal $\mathbf{x}^{(u_{\text{opt}})}$ selected for transmission in M-PTS is the candidate OFDM signal with index $u_{\text{opt},T}$ given by

$$u_{\text{opt},T} = \arg \min_{u=0}^{U-1} \max_{n \in \mathbf{S}_T(\gamma_T)} \left| \sum_{v=0}^{V-1} b_v^{(u)} x_{v,n} \right|^2 . \tag{4.24}$$

Block diagrams of the proposed PTS schemes are shown in Figure 4.4. Figure 4.4(a) illustrates A-PTS while Figure 4.4(b) shows M-PTS.

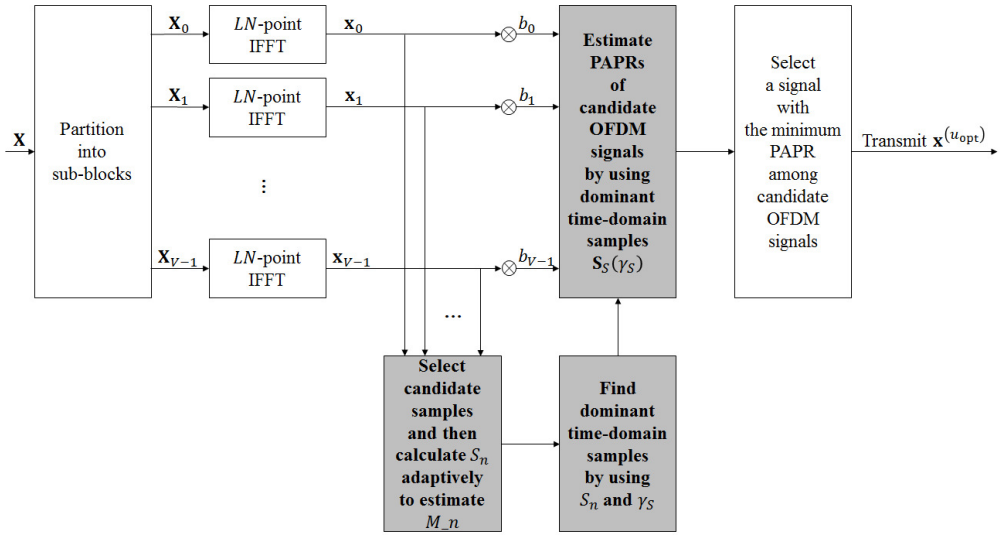

(a) A-PTS

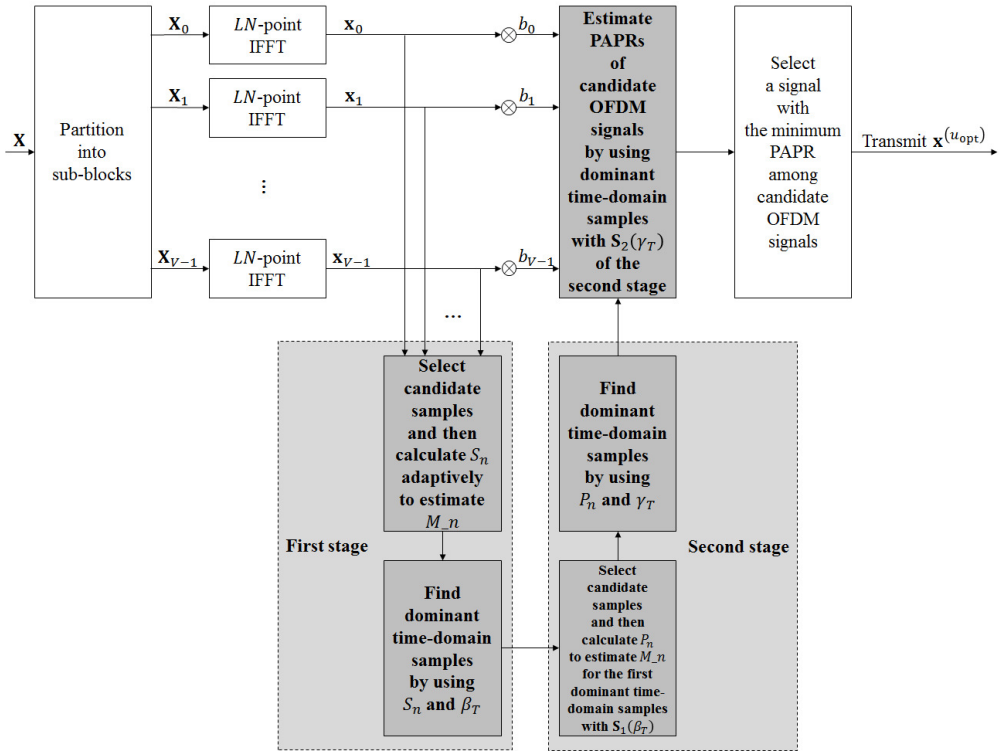

(b) M-PTS

Figure 4.4: Block diagrams of the proposed PTS schemes with adaptive selection methods for dominant time-domain samples.

Chapter 5

PERFORMANCE ANALYSIS

In this chapter, the performances of the proposed PTS schemes, LC-PTS, A-PTS, and M-PTS, are numerically analyzed. First, the computational complexity of the proposed PTS schemes is considered and compared to those of the previously known PTS schemes. In addition, the computational complexity of the proposed PTS schemes with specific parameters is evaluated and compared to those of the previous PTS schemes while maintaining the optimal PAPR reduction performance.

5.1 Computational Complexity

This section compares the computational complexity of the conventional PTS scheme, RC-PTS [23], and the proposed PTS schemes. For comparison, the ratio p_γ is defined as the ratio between the number of selected dominant time-domain samples and the number of total time-domain samples, that is,

$$p_\gamma = \frac{N_\gamma}{LN} \tag{5.1}$$

for A-PTS. Moreover, for the first stage of M-PTS, the ratio p_β is defined as the ratio between the number of selected dominant time-domain samples in the first selection

stage and the number of total time-domain samples given by

$$p_\beta = \frac{N_\beta}{LN}. \tag{5.2}$$

Note that for the second stage of M-PTS, p_γ is also the ratio between the number of selected dominant time-domain samples in the second selection stage and the number of total time-domain samples as given by (5.1).

Table 5.1 compares the computational complexity after IFFT of the conventional PTS, RC-PTS, LC-PTS, IRC-PTS and the proposed PTS schemes using the parameters N, L, V, and W. The parameter p_γ or p_β (N_γ or N_β) is used to represent the computational complexity of the PTS schemes using the dominant time-domain samples. Additionally, the variables C and $C_n, 0 \leq n \leq LN-1$ are used to express the number of searches for the candidate samples at each n in the LC-PTS and in the proposed PTS schemes, respectively. Note that the computational complexity required to check the conditions of the proposed selection methods for the candidate samples is very low and thus it can be ignored. For the specific parameter, the computational complexity of the PTS schemes is described in the next section.

Table 5.1: Computational complexity after IFFT in PTS schemes

PTS schemes	Number of complex multiplications
Conventional PTS [10]	LNU
RC-PTS [23]	$LNV + p_\gamma LNU = LNV + N_\gamma U$
IRC-PTS [24]	$1.25LNV + p_\gamma LNU = 1.25LNV + N_\gamma U$
LC-PTS	$LNC + p_\gamma LNU = LNC + N_\gamma U$
A-PTS	$\sum_{n=0}^{LN-1} C_n + p_\gamma LNU = \sum_{n=0}^{LN-1} C_n + N_\gamma U$
M-PTS	$\sum_{n=0}^{LN-1} C_n + p_\beta LNC + p_\gamma LNU = \sum_{n=0}^{LN-1} C_n + N_\beta C + N_\gamma U$

5.2 Simulation Results

This section compares the PAPR reduction performance of the conventional PTS, RC-PTS, LC-PTS, and the proposed PTS schemes. As explained in Chapter 1, BER is affected only by the PAPR in condition that other system conditions except only for the PAPR of OFDM signals are fixed in OFDM systems. It means that the PAPR reduction performance is directly connected to BER performance and improvement of communication quality in OFDM systems.

Figures 5.1 and 5.2 compare the PAPR reduction performance of the conventional PTS, RC-PTS, IRC-PTS, LC-PTS, A-PTS, and M-PTS in cases with 16-QAM, $L = 4$, $V = 8$, and $W = 2$, where $N = 256$ and 1024 are considered, respectively. Note that IRC-PTS is simulated by using the scheme Proposed(Y) [24]. For a fair comparison, N_γ and the corresponding p_γ (N_β and the corresponding p_β) are set in each PTS scheme except for the conventional PTS schemes, such that they achieve the optimal PAPR reduction performance with their respective minimum values of N_γ and p_γ (N_β and the corresponding p_β), which is identical to that by the conventional PTS. Note that the respective minimum values of N_γ and p_γ in those PTS schemes for the optimal PAPR reduction performance are obtained by exhaustive searches. Therefore, those PTS schemes achieve the optimal PAPR reduction performance, but their required N_γ and p_γ differ.

For $N = 256$ as shown in Figure 5.1, the N_γ's for RC-PTS, IRC-PTS, LC-PTS, and A-PTS are 56, 36, 15, and 51, respectively. Therefore, the corresponding p_γ's are 0.055, 0.035, 0.015, and 0.05. Furthermore, N_β and N_γ of M-PTS are 51 and 15, respectively, where the corresponding values of p_β and p_γ are 0.05 and 0.015, when $N = 256$, as shown in Figure 5.1.

For $N = 1024$ as shown in Figure 5.2, the N_γ's for RC-PTS, IRC-PTS, LC-PTS and A-PTS are 102, 45, 16, and 164, respectively. Therefore, the corresponding p_γ's are 0.025, 0.011, 0.004, and 0.04. In addition, N_β and N_γ of M-PTS are 143 and 16, where the corresponding values of p_β and p_γ are 0.035 and 0.004, respectively when

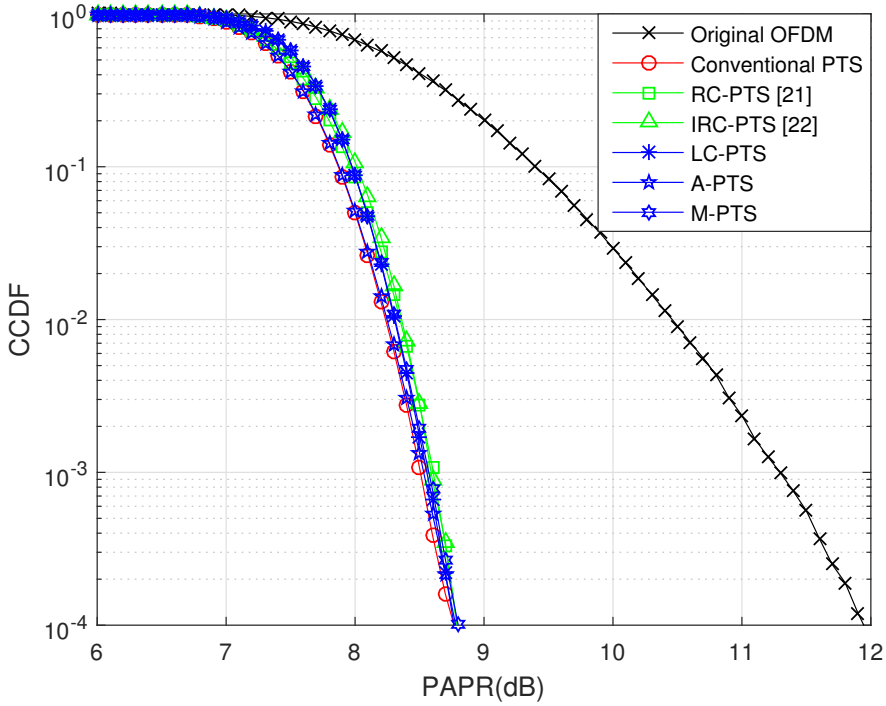

Figure 5.1: PAPR reduction performance of PTS schemes for $N = 256$, 16-QAM, $L = 4$, $V = 4$, and $W = 2$.

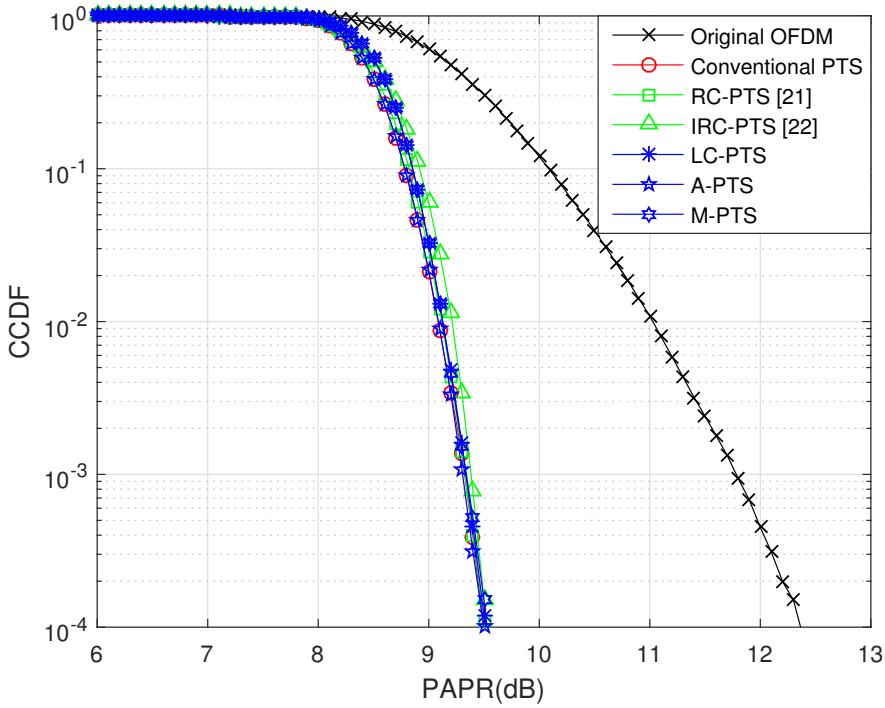

Figure 5.2: PAPR reduction performance of PTS schemes for $N = 1024$, 16-QAM, $L = 4$, $V = 4$, and $W = 2$.

$N = 1024$ as shown in Figure 5.2.

Tables 5.2 and 5.3 compare the computational complexity of those PTS schemes for cases of 16-QAM, $L = 4$, $V = 4$, and $W = 2$, where $N = 256$ and 1024 as shown in Figures 5.1 and 5.2, respectively. As indicated in Figures 5.1 and 5.2, N_γ and the corresponding p_γ (N_β and the corresponding p_β) are set in each PTS scheme except for the conventional PTS scheme in Tables 5.2 and 5.3 respectively such that they achieve the optimal PAPR reduction performance with their minimum values of N_γ and p_γ (N_β and the corresponding p_β), identical to that of the conventional PTS.

Table 5.2: Computational complexity after IFFT in PTS schemes for $N = 256$, 16-QAM, $L = 4$, $V = 4$, and $W = 2$

PTS schemes	Number of complex multiplications
Conventional PTS	8192 (100%)
RC-PTS [23] ($N_\gamma = 56$, $p_\gamma = 0.055$)	4216 (55.5%)
IRC-PTS [24] ($N_\gamma = 36$, $p_\gamma = 0.035$)	5328 (65.0%)
LC-PTS ($N_\gamma = 15$, $p_\gamma = 0.015$)	4216 (51.5%)
A-PTS ($N_\gamma = 51$, $p_\gamma = 0.05$)	1821 (22.2%)
M-PTS ($[N_\beta, N_\gamma] = [51, 15]$, $[p_\beta, p_\gamma] = [0.05, 0.015]$)	1737 (21.2%)

In Table 5.2, the computational complexity of those PTS schemes is compared for cases of $N = 256$, 16-QAM, $L = 4$, $V = 4$, and $W = 2$ as shown in Figure 5.1. Compared to the conventional PTS, A-PTS and M-PTS show much lower and the lowest computational complexity of 22.2% and 21.2%, respectively, while achieving the identical PAPR value of 8.7dB when CCDF $= 10^{-4}$, which means the optimal

Table 5.3: Computational complexity after IFFT in PTS schemes for $N = 1024$, 16-QAM, $L = 4$, $V = 4$, and $W = 2$

PTS schemes	Number of complex multiplications
Conventional PTS	32768 (100%)
RC-PTS [23] ($N_\gamma = 102$, $p_\gamma = 0.025$)	17200 (52.5%)
IRC-PTS [24] ($N_\gamma = 45$, $p_\gamma = 0.011$)	20840 (63.6%)
LC-PTS ($N_\gamma = 16$, $p_\gamma = 0.004$)	16512 (50.4%)
A-PTS ($N_\gamma = 164$, $p_\gamma = 0.04$)	6964 (21.3%)
M-PTS ($[N_\beta, N_\gamma] = [143, 16]$, $[p_\beta, p_\gamma] = [0.035, 0.004]$)	6352 (19.4%)

PAPR reduction performance for cases of $N = 256$, as shown in Figure 5.1. Also, LC-PTS shows considerably low computational complexity of 51.5% while maintaining the optimal PAPR reduction performance. On the other hand, RC-PTS and IRC-PTS show higher computational complexity of 55.5% and 65.0% with the optimal PAPR reduction performance, respectively compared to the proposed PTS schemes.

Additionally, Table 5.3 compares the computational complexity of those PTS schemes for cases of $N = 1024$, 16-QAM, $L = 4$, $V = 4$, and $W = 2$ as shown in Figure 5.2. Compared to the conventional PTS, A-PTS and M-PTS show much lower and the lowest computational complexity of 21.3% and 19.4%, respectively, while maintaining an identical PAPR value of 9.5dB when CCDF $= 10^{-4}$, which represents the optimal PAPR reduction performance for $N = 1024$ as shown in Figure **??**. In addition, LC-PTS shows reduced computational complexity of 50.4% while achieving the optimal PAPR reduction performance. On the other hand, RC-PTS and IRC-PTS

show corresponding computational complexity of 52.5% and 63.6% with the optimal PAPR reduction performance, respectively compared to the proposed PTS schemes.

Figures 5.3 and 5.4 compare the PAPR reduction performance of the conventional PTS, RC-PTS, IRC-PTS, LC-PTS, and A2-PTS for cases of 16-QAM, $L = 4$, $V = 8$, and $W = 2$, where $N = 256$ and $N = 1024$ are considered, respectively. For a fair comparison as in Figures 5.3 and 5.4, N_γ and the corresponding p_γ are set in each PTS scheme except for the conventional PTS scheme, such that they achieve the optimal PAPR reduction performance with their respective minimum values of N_γ and p_γ. Note that the conventional PTS scheme also achieves the optimal PAPR reduction performance. For $N = 1024$, those PTS schemes achieve the optimal PAPR reduction performance but their required N_γ and p_γ differ. However, for $N = 256$, RC-PTS and IRC-PTS cannot achieve the optimal PAPR reduction performance with even high values of N_γ ($= 512$) and p_γ ($= 0.5$), while the other PTS schemes do achieve this level of performance given their differently required values of N_γ and p_γ.

For $N = 256$ as shown in Figure 5.3, the N_γ's of the RC-PTS, IRC-PTS, LC-PTS, and A2-PTS are 512, 225, 225, and 512, respectively. Hence, the corresponding p_γ's are 0.5, 0.5, 0.22, and 0.22. Moreover, for $N = 1024$ as shown in Figure 5.4, the N_γ's of RC-PTS, IRC-PTS, LC-PTS, and A2-PTS are 1730, 1311, 348, and 348, respectively. Therefore, the corresponding p_γ's are 0.42, 0.32, 0.085, and 0.085.

Tables 5.4 and 5.5 compare the computational complexity of those PTS schemes for cases of 16-QAM, $L = 4$, $V = 8$, and $W = 2$, where $N = 256$ and 1024 as shown in Figures 5.1 and 5.2, respectively. As indicated in Figures 5.1 and 5.2 similar to case of $V = 4$, N_γ and the corresponding p_γ are set differently in each PTS scheme, except for the conventional PTS schemes in Tables 5.4 and 5.5.

In Table 5.4, the computational complexity of those PTS schemes is compared for cases of $N = 256$, 16-QAM, $L = 4$, $V = 8$, and $W = 2$ as shown in Figure 5.3. Compared to the conventional PTS, LC-PTS and A2-PTS show much lower and the lowest computational complexity of 25.1% and 24.8%, respectively while

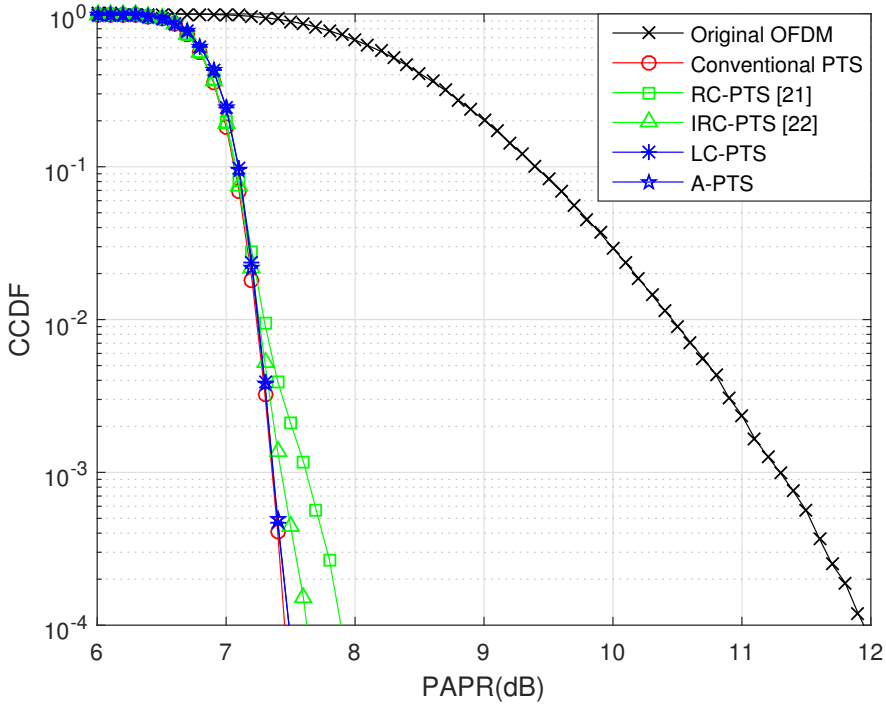

Figure 5.3: PAPR reduction performance of PTS schemes for $N = 256$, 16-QAM, $L = 4$, $V = 8$, and $W = 2$.

Table 5.4: Computational complexity after IFFT in PTS schemes for $N = 256$, 16-QAM, $L = 4$, $V = 8$, and $W = 2$

PTS schemes	Number of complex multiplications
Conventional PTS	131072 (100%)
RC-PTS [23] ($N_\gamma = 512$, $p_\gamma = 0.5$)	73728 (56.3%)
IRC-PTS [24] ($N_\gamma = 512$, $p_\gamma = 0.5$)	75776 (57.8%)
LC-PTS ($N_\gamma = 225$, $p_\gamma = 0.22$)	32896 (25.1%)
A2-PTS ($N_\gamma = 225$, $p_\gamma = 0.22$)	32470 (24.8%)

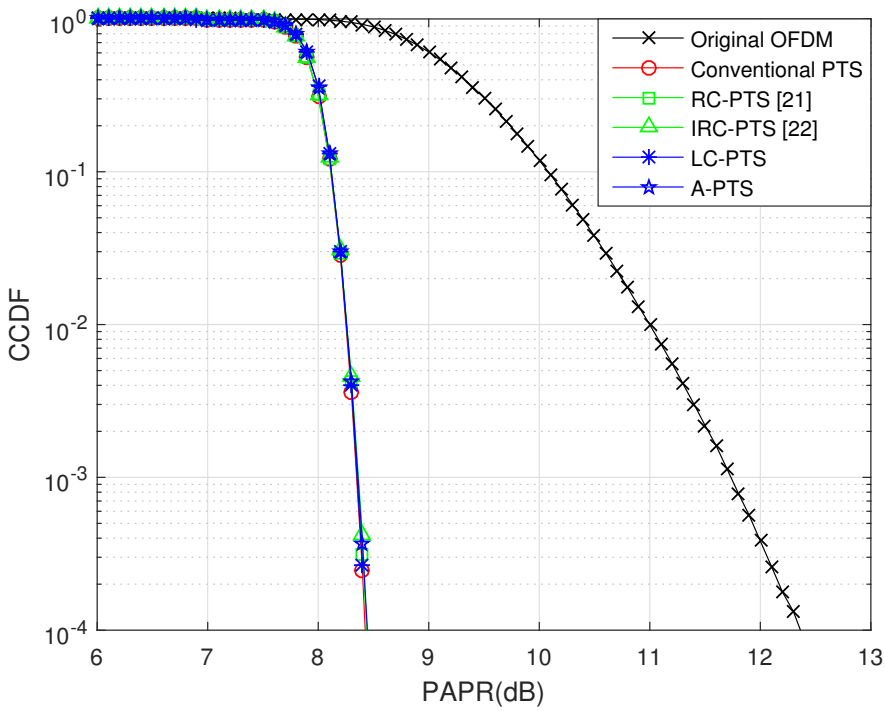

Figure 5.4: PAPR reduction performance of PTS schemes for $N = 1024$, 16-QAM, $L = 4$, $V = 8$, and $W = 2$.

Table 5.5: Computational complexity after IFFT in PTS Schemes for $N = 1024$, 16-QAM, $L = 4$, $V = 8$, and $W = 2$

PTS schemes	Number of complex multiplications
Conventional PTS	524288 (100%)
RC-PTS [23] ($N_\gamma = 1720$, $p_\gamma = 0.42$)	252928 (48.2%)
IRC-PTS [24] ($N_\gamma = 1311$, $p_\gamma = 0.32$)	208768 (39.8%)
LC-PTS ($N_\gamma = 348$, $p_\gamma = 0.085$)	60928 (11.6%)
A2-PTS ($N_\gamma = 348$, $p_\gamma = 0.085$)	59225 (11.3%)

achieving the identical PAPR of 7.5dB at CCDF $= 10^{-4}$, which represents the optimal PAPR reduction performance for cases of $N = 256$, as shown in Figure 5.3. On the other hand, RC-PTS and IRC-PTS show computational complexity of 56.3% and 57.8%, respectively. Note that RC-PTS and IRC-PTS cannot achieve the optimal PAPR reduction performance with even higher computational complexity compared to the proposed PTS schemes.

In addition, Table 5.5 compares the computational complexity of those PTS schemes for cases of $N = 1024$, 16-QAM, $L = 4$, $V = 8$, and $W = 2$ as shown in Figure 5.4. Compared to the conventional PTS, LC-PTS and A2-PTS shows much lower and the lowest computational complexity of 11.6% and 11.3%, respectively while achieving the identical PAPR value of 8.4dB when CCDF $= 10^{-4}$, which shows the optimal PAPR reduction performance for cases with $N = 1024$ as shown in Figure 5.4. On the other hand, RC-PTS and IRC-PTS show corresponding computational complexity of 48.2% and 39.8% with the optimal PAPR reduction performance, respectively compared to the proposed PTS schemes.

Chapter 6

CONCLUSIONS

In this dissertation, we reviewed OFDM systems and the PAPR characteristics of OFDM signals. To overcome the PAPR problem of OFDM systems, many PAPR reduction schemes have been proposed. PTS schemes are a kind of solutions among them and have efficient characteristics and high PAPR reduction performance. However, high computational complexity is one of the most significant drawbacks of the PTS schemes. In order to reduce computational complexity of the PTS schemes, several modified PTS schemes have been proposed but their computational complexities are still high. The PTS schemes proposed in this dissertation lower computational complexity of the previous PTS schemes considerably while maintaining the optimal PAPR reduction performance.

In Chapter 3, LC-PTS is proposed to reduce the computational complexity. The computational complexity for calculating PAPRs of candidate OFDM signals is reduced by selecting dominant time-domain samples using new method to select candidate samples for estimating maximum power of time-domain samples. Based on the proposed selection method for candidate samples and the corresponding selection method for dominant time-domain samples, LC-PTS is proposed to reduce computational complexity while maintaining the optimal PAPR reduction performance.

In Chapter 4, in order to reduce the computational complexity of the previous PTS

schemes further, additional three low-complexity PTS schemes are proposed. Although the proposed PTS schemes use dominant time-domain samples similar to the previous low-complexity PTS schemes, more efficient selection methods for the dominant time-domain samples are proposed. A1-SM and A2-SM are new methods to select candidate samples adaptively for estimating maximum power of time-domain samples and then selecting dominant time-dominant samples. Also, M-SM is a multi-stage method to select dominant time-domain samples. A1-SM, A2-SM, and M-SM can reduce the computational complexity required for calculating the PAPRs of candidate OFDM signals considerably compared to the previous PTS schemes. Based on A1-SM, A2-SM, and M-SM, new PTS schemes A-PTS and M-PTS are proposed for performance enhancement in terms of computational complexity and PAPR reduction.

In Chapter 5, the performances of the proposed PTS schemes, LC-PTS, A-PTS, and M-PTS, are numerically analyzed in terms of computational complexity and PAPR reduction. The proposed PTS schemes can reduce the computational complexity considerably while achieving optimal PAPR reduction performance. Therefore, the proposed PTS schemes are promisingly expected to be used as the PAPR reduction scheme of the OFDM signals in the practical implementation of OFDM systems.

Bibliography

[1] R. W. Chang and R. A. Gibby, "A theoretical study of performance of an orthogonal multiplexing data transmission scheme," *IEEE Transactions on Communications*, vol. 16, no. 4, pp. 529-540, August 1968.

[2] IEEE Std. 802.11g-2003, Part 11: Wireless LAN Medium Access Control (MAC) and Physical Layer (PHY) specifications amendment 4: further higher data rate extension in the 2.4 GHz band, IEEE Std. 802.11g, 2003 edition, 2003.

[3] R. Gross and D. Veeneman, "Clipping distortion in DMT ADSL systems," *Electronics Letters*, vol. 29, no. 24, pp. 2080–2081, November 1993.

[4] X. Li and L. J. Cimini, Jr., "Effect of clipping and filtering on the performance of OFDM," *IEEE Communications Letters*, vol. 2, no. 5, pp. 131–133, May 1998.

[5] X. Wang, T. T. Tjhung, and C. S. Ng, "Reduction of peak-to-average power ratio of OFDM system using a companding technique," *IEEE Transactions on Broadcasting*, vol. 45, no. 3, pp. 303–307, September 1999.

[6] J. Tellado, "Peak to Average Power Reduction for Multicarrier Modulation," Ph.D. Dissertation, EE Department, Stanford Univ., 2000.

[7] B. S. Krongold and D. L. Jones, "PAR reduction in OFDM via active constellation extension," *IEEE Transactions on Broadcasting*, vol. 49, no. 3, pp. 258–268, September 2003.

[8] A. E. Jones, T. A. Wilkinson, and S. K. Barton, "Block coding scheme for reduction of peak to mean envelope power ratio of multicarrier transmission scheme," *Electronics Letters*, vol. 30, no. 22, pp. 2098–2099, December 1994.

[9] R. W. Baüml, R. F. H. Fischer, and J. B. Huber, "Reducing the peak-to-average power ratio of multicarrier modulation by selected mapping," *Electronics Letters*, vol. 32, no. 22, pp. 2056–2057, October 1996.

[10] S. H. Müller and J. B. Huber, "OFDM with reduced peak-to-average power ratio by optimum combination of partial transmit sequences," *Electronics Letters*, vol. 33, no. 5, pp. 368–369, February 1997.

[11] D.-W. Lim, H.-S. Noh, J.-S. No, and D.-J. Shin, "Near optimal PRT set selection algorithm for tone reservation in OFDM systems," *IEEE Transactions on Broadcasting*, vol. 54, no. 3, pp. 454–460, September 2008.

[12] D.-W. Lim, H.-S. Noh, H.-B. Jeon, J.-S. No, and D.-J. Shin, "Multi-stage TR scheme for PAPR reduction in OFDM signals," *IEEE Transactions on Broadcasting*, vol. 55, no. 2, pp. 300–304, June 2009.

[13] L. J. Cimini and N. R. Sollenberger, "Peak-to-average power ratio reduction of an OFDM signal using partial transmit sequences," *IEEE Communications Letters*, vol. 4, no. 3, pp. 86–88, March 2000.

[14] A. Alavi, C. Tellambura, and I. Fair, "PAPR reduction of OFDM signals using partial transmit sequence: An optimal approach using sphere decoding," *IEEE Communications Letters*, vol. 9, no. 11, pp. 982–984, November 2005.

[15] T. T. Nguyen and L. Lampe, "On partial transmit sequences for PAR reduction in OFDM system," *IEEE Transactions on Wireless Communications*, vol. 7, no. 2, pp. 746–755, February 2008.

[16] J.-H. Wen, S.-H. Lee, and Y.-F. Huang, "A suboptimal PTS algorithm based on particle swarm optimization for PAPR reduction in OFDM systems," *EURASIP Journal on Wireless Communications and Networking*, vol. 2008, no. 14, pp. 1–8, May 2008.

[17] D.-W. Lim, S.-J. Heo, J.-S. No, and H. Chung, "A new PTS OFDM scheme with low complexity for PAPR reduction," *IEEE Transactions on Broadcasting*, vol. 52, no. 1, pp. 77–82, March 2006.

[18] Y. Wang, W. Chen, and C. Tellambura, "A PAPR reduction method based on artificial bee colony algorithm for OFDM signals," *IEEE Transactions on Wireless Communications*, vol. 9, no. 10, pp. 2994–2999, October 2010.

[19] R. Ruo, C. Zhang, N. Niu, and R. Li, "A low-complexity PTS based on greedy and genetic algorithm for OFDM systems," *Chinese Journal of Electronics*, vol. 24, no. 4, pp. 857–861, October 2015.

[20] J. Zhou, E. Dutkiewicz, R. P. Liu, X. Huang, G. Fang, and Y. Liu, "A modified shuffled frog leaping algorithm for PAPR reduction in OFDM systems," *IEEE Transactions on Broadcasting*, vol. 61, no. 4, pp. 698–709, October 2015.

[21] Y.-J. Cho, J.-S. No, and D.-J. Shin, "A new low-complexity PTS scheme based on successive local search using sequences," *IEEE Communications Letters*, vol. 16, no. 9, pp. 1470–1473, September 2012.

[22] K.-H. Kim, "On the shift value set of cyclic shifted sequences for PAPR reduction in OFDM systems," *IEEE Transactions on Broadcasting* vol. 62, no. 2, pp. 496–500, June 2016.

[23] S.-J. Ku, C.-L. Wang, and C.-H. Chen, "A reduced-complexity PTS-based PAPR reduction scheme for OFDM systems," *IEEE Transactions on Wireless Communications*, vol. 9, no. 8, pp. 2455–2460, August 2010.

[24] Y.-C. Cho, K.-H. Kim, J.-Y. Woo, K.-S. Lee, J.-S. No, and D.-J. Shin, "Low-complexity PTS schemes using dominant time-domain samples in OFDM systems," *IEEE Transactions on Broadcasting*, vol. 63, no. 2, pp. 440–445, March 2017.

[25] C. Tellambura, "Computation of the continuous time PAR of an OFDM signal with BPSK subcarriers," *Electronics Letters*, vol. 5, no. 5, pp. 185–87, May 2001.

[26] A. A. M. Saleh, "Frequency-independent and frequency-dependent nonlinear models of TWT amplifiers," *IEEE Transactions on Communications*, vol. 29, no. 11, pp. 1715–1720, November 1981.

[27] C. Rapp, "Effects of HPA nonlinearity on a 4-DPSK/OFDM signal for a digital sound broadcasting system," *In ESA, Second European Conference on Satellite Communications*, pp. 179–184, October 1991.

[28] H. Ochiai, "Performance analysis of peak power and band-limited OFDM system with linear scaling," *IEEE Translations on Wireless Communications*, vol. 2, no. 5, pp. 1055–1065, September 2003.

[29] C. Tellambura, "Use of m-sequence for OFDM peak-to-average power ratio reduction," *Electronics Letters*, vol. 33, no. 15, pp. 1300–1301, July 1997.

[30] C. Tellambura, "Phase optimization criterion for reducing peak-to-average power ratio in OFDM," *Electronics Letters*, vol. 34, no. 2, pp. 169–170, January 1998.

[31] D. Dardari, V. Tralli, and A. Vaccari, "A theoretical characterization of nonlinear distortion effects in OFDM systems," *IEEE Transactions on Communications*, vol. 48, no. 10, pp. 1755–1764, October 2000.

[32] D.-W. Lim, C.-W. Lim, J.-S. No, and H. Chung, "A new SLM OFDM with low complexity for PAPR reduction," *IEEE Signal Processing Letters*, vol. 12, no. 2, pp. 93–96, February 2005.

[33] S.-J. Heo, H.-S. Noh, J.-S. No, and D.-J. Shin, “A modified SLM scheme with low complexity for PAPR reduction of OFDM systems,” *IEEE Transactions on Broadcasting*, vol. 53, no. 4, pp. 804–808, December 2007.

초 록

직교주파수분할다중화 (OFDM) 시스템에서 직교주파수분할다중화 신호의 높은 최대전력대평균전력비 (PAPR)는 해결하여야 가장 중요한 문제들 중 하나이다. 직교주파수분할다중화 신호의 높은 최대전력대평균전력비는 신호가 고출력증폭기 (HPA)를 통과할 때 심각한 비선형 왜곡을 발생시킨다. 이러한 왜곡들은 대역내 왜곡과 대역외 신호를 발생시키는데, 이들은 각각 수신된 신호의 비트오류율 (BER) 성능 열화와 인접 채널 간섭에 영향을 미친다. 직교주파수분할다중화 신호의 최대전력대평균전력비 문제를 해결하기 위해 다양한 최대전력대평균전력비 감소 기법들이 제안되어 왔다.

본 논문은 직교주파수분할다중화 시스템의 최대전력대평균전력비 감소 기법 중 하나인 부분전송수열 (PTS) 기법 연구에 관한 내용이다. 부분전송수열 기법은 높은 최대전력대평균전력비 감소 성능과 신호 왜곡이 없는 특성 때문에 직교주파수분할다중화 시스템의 최대전력대평균전력비 문제에 대한 해결책으로 매우 적합한 기법이다. 부분전송수열 기법은 기존 직교주파수분할다중화 신호를 표현할 수 있는 여러 개의 후보 신호들을 발생시키고, 이들 중 가장 낮은 최대전력대평균전력비를 갖는 신호를 전송 신호로 선택한다. 그러나 부분전송수열 기법을 사용하는데 있어서, 후보 신호들을 발생시키고 처리하는데 필요한 높은 계산 복잡도는 심각한 문제가 될 수 있다. 본 논문에서는, 부분전송수열 기법의 계산 복잡도를 감소시키기 위해 시간 영역의 큰 샘플들을 선별하여 활용하는 새로운 부분전송수열 기법들을 제안한다. 시간 영역의 큰 샘플들은 후보 신호들의 최대전력대평균전력비를 효율적으로 추정하기 위해 사용되는 직교주파수분할다중화 신호의 소수 샘플들을 의미한다.

첫번째로 본 논문에서는, 시간 영역의 큰 샘플의 새로운 선별 방법들을 사용하는 저복잡도 부분전송수열 기법들을 제안한다. 제안된 선별 방법들은 후보 신호들의 후보 샘플들의 선택 방법들을 기반으로 한다. 후보 샘플들의 선택 방법들은 감소된 복잡도로 시간 영역의 큰 샘플들을 선별할 수 있다. 이 방법들로 선별된 시간 영역의 큰 샘플들은 높은 추정 성능으로 후보 신호들의 최대전력대평균전력비를 추정하는데 사용된다. 따라서 제안된 저복잡도 부분전송수열 기법들은 상당히 감소된 계산복잡도로도 최적의 최대전력대평균전력비 감소 성능을 달성할 수 있다.

다음으로 본 논문에서는, 높은 최대전력대평균전력비 감소 성능을 유지하면서 계산복잡도를 더 줄이기 위해, 개선된 부분전송수열 기법을 제안한다. 이 부분전송수열 기법들은 첫번째로 제안된 기법들과 유사하게 시간 영역의 큰 샘플들과 후보 샘플들을 활용한다. 그러나 개선된 부분전송수열 기법들은 더 효율적인 선별 방법들을 사용하는데, 이들은 시간 영역의 큰 샘플들을 선별하기 위해 적응 방법 또는 다단계 방법을 사용하여 후보 샘플들을 선택한다. 따라서 이 부분전송수열 기법들은 최적의 최대전력대평균전력비 감소 성능을 유지하면서 계산 복잡도를 추가적으로 감소시킬 수 있다.

본 논문에서 제안된 부분전송수열 기법들은 시간 영역의 큰 샘플들을 선별하기 위해 효율적인 선택 방법을 사용한다. 제안된 부분전송수열 기법들은 기존의 부분전송수열 기법들과 비교하여 최적의 최대전력대평균전력비 감소 성능을 달성하면서 계산 복잡도를 상당히 감소시킨다. 따라서 제안된 부분전송수열 기법들은 높은 성능과 낮은 복잡도의 장점으로 인해 실제 구현되는 직교주파수분할다중화 시스템에 사용 가능할 것으로 기대된다.

주요어: 부분전송수열, 직교주파수분할다중화, 최대전력대평균전비
학번: 2012-20821